iscte

INSTITUTO
UNIVERSITÁRIO
DE LISBOA

USV Charging Based on WPT System

Chen Ye

Master in Telecommunications and Computer Engineering

Supervisors:
Dr. Octavian Postolache, Associate Professor with Habilitation
ISCTE-Instituto Universitario de Lisboa

Prof. Dr. Wangqiang Niu, Associate Professor,
Shanghai Maritime University

November, 2020

iscte

**TECNOLOG|AS
E ARQU|TETURA**

Science and Information Technology Department

USV Charging Based on WPT System

Chen Ye

Master in Telecommunications and Computer Engineering

Supervisors:
Prof. Dr. Octavian Postolache, Associate Professor with Habilitation
ISCTE-Instituto Universitario de Lisboa

Prof. Dr. Wangqiang Niu, Associate Professor,
Shanghai Maritime University

November, 2020

Acknowledgments

This Master's dissertation has received much important support from which I am grateful. The encouragement, participation and collaboration with the professors help me realize this project.

Finally, I thank my parents for their unconditional support. I especially dedicate this project to all those who directly or indirectly contributed to the success of this research. To all my sincere thanks.

Resumo

Com a crescente procura da exploração em ambientes aquáticos e subaquáticos , os veículos elétricos de superfície não tripulados ("electric unmanned surface vehicle" -USV) têm sido cada vez mais utilizados nestes últimos anos. No entanto, devido aos limites atuais relacionados com a tecnologia utilizada nas baterias, os dispositivos precisam de ser recarregados com frequência para poderem operar num ambiente aquático complexo. Para melhorar a segurança e a conveniência do carregamento da bateria de um USV, um sistema para recarregamento da bateria de um barco não tripulado através de transferência de energia sem fios ("wireless power transfer" - WPT) é proposto nesta dissertação. Neste caso de estudo, o barco tem a capacidade de ser controlado para chegar a um ponto de recarregamento da bateria, que se encontra fixado por uma doca mecânica. Enquanto o sistema WPT é recarregado, os dados associados ao processo de recarregamento da bateria podem ser monitorizados por um computador host.

O controlo da movimentação do barco é baseado num sistema embebido. A posição relativa entre a bobina transmissora e a bobina receptora deve ser detectada pelo sensor magnético, uma vez que a posição relativa tem um grande impacto na eficiência da transmissão.

Em termos do computador host, foi utilizado o software LABVIEW para programar a interface que permite controlar o movimento do barco e recolher os dados. Finalmente, a eficácia do sistema proposto foi experimentada e testada num ambiente de laboratório.

Palavras-Chave: Veículo Aquático Não Tripulado; Sistema de transferência de energia sem fios; Eletrónica de potência; Carregamento de tensão constante; Interface LABVIEW

Abstract

With the increasing demand of water and underwater exploration, more and more electric unmanned surface vehicles (USV) are put into use in recent years. However, because of the present battery technology limits, these devices require to be recharged frequently that is a challenging problem taking into account the complex water environment where these equipments are acting. To improve safety and convenience of USV charging a wireless power transfer (WPT) system is proposed in this dissertation. In this case, the boat can be controlled to go to the charging facilities. During charging by the implemented WPT system, the state of charging can be remotely monitored by host computer.

The moving control is based on embedded system. The relative position between transmitting coil and receiving coil is supposed to be sensed by magnetic sensor, since the relative position has great impact on transmission efficiency.

The remote monitoring software was implemented in the host computer and was developed in LABVIEW. A graphical user interface was developed to control the boat moving and collect the data from the WPT and the boat sensors. The effectiveness of the proposed system was tested for instance in the laboratory environment and in-field tests are also planned in the near future.

Keywords: Unmanned Water Vehicle; Wireless Power Transfer System; Power Electronics; Constant Voltage Charging; LABVIEW Graphical User Interface

Contents

Tables

Figures

List of Acronyms

WPT – Wireless Power Transfer

UWPT – Underwater Wireless Power Transfer

USV – Unmanned Surface Vehicle

UAV – Underwater Autonomy Vehicle

IPT – Inductive Power Transfer

MV – Manned Vehicle

ARROS – Algal Bloom Removal Robotic System

NSB – Null-space-based Behavioral

MUSV – Multiple Unmanned Surface Vehicle

GPS – Global Positioning System

OA – Obstacle Avoidance

AIS – Automatic Identification System

DOF – Degrees of Freedom

PC – Personal Computer

FFD – Full Function Device

RFD – Reduced Function Device

RF – Radio Frequency

TTL – Transistor–transistor Logic

Etc.

Chapter 1 – Introduction

1.1. Motivation

Nowadays, as the whole world put more emphasis on ocean resource exploration, water environment monitoring and protection, the usage of unmanned water and under water vehicles become frequently used solution. During in-field usage of those water or underwater equipments, some problems usually occur in conventional charging which requires wired electrical connections. For instance, the environment with high humidity and salinity may cause metal charging connectors rusty or even a short circuit. In addition, frequent plugging may shorten life of connectors, which also reduces safety and dependency of charging. Although there's another solution that replaces the battery on the shore, it still lacks convenience and decreases working efficiency. As a result, wireless power transfer technology comes into view and arouses more and more interests of scientists and engineers [1].

WPT which is firstly proposed by American scientist Nikola Tesla in 1899 is a kind of technology which enables load devices to gain electric power from power source in a contactless way. It can be realized mainly by three ways which are electromagnetic induction transmission, laser transmission and sonic transmission. [2] However, the most common and simplest to achieve one is electromagnetic inductive wireless power transfer which can significantly increase convenience, safety and dependency of charging for USV [3-4].

This proposal aims to mainly use WPT technology to increase performance and improve the usage of USV in different applications such as water quality monitoring considering its endurance. Besides, many other technologies including motor control, electromagnetic sensing, wireless communication and balance charging are considered as compoennets of USV system [5-6]. The motion track of the boat is controlled by the host computer which is also able to read data of battery and status of motion wirelessly. Finally, during process of charging, the charging time and efficiency will be measured taking into account that are essential on power transmission effectiveness [7-9].

1.2. Objectives

In this work it is proposed to integrate WPT system with the unmanned water vehicle considering the development of specific hardware and software. The goal is to implement the basic functions which involve sonic obstacle avoiding, data transmission, as well as

battery state monitoring and wireless charging which is the core of the research. In order to guarantee that whole system is working effectively, it's important to consider the practical applying condition since the USV is designed to work for relatively long periods on water.

The ideal operation of the USV is described below: When the battery power of the USV is over the safe value, which means that the voltage of each cell of the 3C Li-Po battery is over 3.0 V, the USV can perform regular tasks such as obstacle avoiding and air quality detection. Once it's detected that one of the cell's voltage reduces to safe value, the host computer will receive the message to remind operator to drive the USV back to the charging station. All data will be wiresly transferred to host computer through APC 220 wireless data transmission module.

As the focal point of the research, the data related to charging is analyzed, including time cost of fully charged, charging rate and efficiency, battery temperature. Considering that the battery in the USV is composed of three cells, it is essential to fully charge all cells to prevent each of them from over charged, which assures long battery life. As a result of utilizing WPT, the charging process for USV can be more flexible and reliable.

As a technology which can enhance charging safety and flexibility, wireless power transfer (WPT) was applied in some high-tech equipment, especially in aquatic drones, considering its complex charging environment. In order to improve the stability of wireless power transfer system voltage output, while the relative position of two coils is changing, a WPT circuit which can supply stable 12 V output voltage and variable current was designed. In this system the distance between transmitting coil (Tx) and receiving coil (Rx) is changing between 5 mm to 30 mm. To get the maximum transmission efficiency, the system is supposed to keep working at resonant frequency which is realized by frequency control chips for inverter in first side and rectifier in second side respectively. The detailed study of battery charging current versus coil distance is analyzed by simulation and experiment. In addition, the parameters of different circuit components such like capacity and inductance are fixed to obtain the resonance, which is determined by calculation and simulation. Meanwhile, the shape of coils is considered as well because it has clear affection on mutual inductance.

1.3.   Structure of the Dissertation

This dissertation is organized in 5 chapters, where different phases of the development of this system and its experimental results are described.

- In Chapter 2, focusses on literature review on the different topics and technologies used to develop this system.

- Chapter 3 describes the whole system's architecture, presenting detailed descriptions of every developed node of the wireless sensor network.

- Chapter 4   gives the methodology of the system design.

- Chapter 5 is the experimental results and discussion.

- In Chapter 6, the conclusions and future work are presented.

Chapter 2 – State of the Art

In this chapter, the various research topics relevant to develop the proposed work are presented. In Section 2.1, the wireless power transfer historical facts and main advantages of WPT for USV is presented compared with the conventional power transfer are presneted. In Section 2.2, the application prospects of USV and some technical problems are introduced. In Section 2.3, some wireless communication protocol is introduced, followed by Section 2.4, where introduces several key hardware components. In Section 2.5, the background of Lithium Polymer (LiPo) battery and its charging is given while Section 2.6 introduced host computer software mainly about LabVIEW.

2.1.1. Wireless power transfer (WPT)

With the great development of electric age, people now have much higher requirements on electric power transmission to cope with various kinds of electricity consumption scenarios, particularly for those mobile electrical appliances which need to work for long time and are limited by battery performance. Then, WPT technology seems to be an ideal solution. Wireless power transfer firstly proposed by Serbian-American scientist Nikola Tesla [10] in 1899 is a technology which enables devices to gain electric power from power source in a contactless way. However, this technology hasn't been widely applied until the last ten years and arouses more and more researchers' interests. Nowadays, WPT is used in robotics, small household appliances, human implant devices, mobile communication devices and electric vehicles, water and underwater unmanned vehicles, etc. Since the present battery life is still not long enough and devices need to be charged frequently, inductive WPT is able to improve safety and convenience of charging because it doesn't need any electrical contact compared with conventional wired power transfer [11]-[13]. Figure 1 shows a common WPT cicuit diagram.
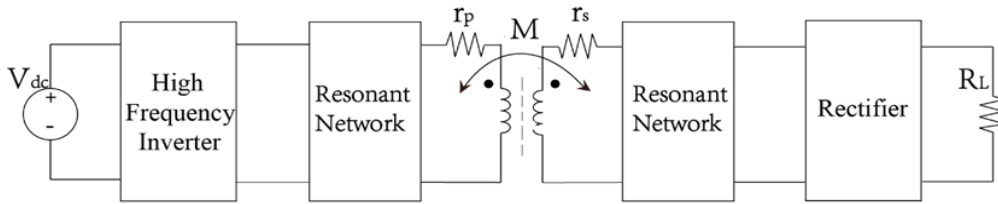
Figure 1 — WPT circuit

2.1.1. The limits remained in WPT and presented solutions

WPT technology is still facing a lot of problems. For instance, WPT efficiency decreases significantly caused by Tx-Rx coils misalignment and the distance between them [14]. To solve the problem, different solutions were presented by researchers. In [15], a dipole-coil-based inductive power transfer (IPT) with a reflector, which adopts the variable switched capacitance under wide-range distance variation between Tx and Rx, is proposed. Unfortunately, in term of coil and circuit volume control, it is sacrificed for transmission performance so that the system lacks practicality. Furthermore, there're many other solutions focusing on coil shape, magnetic or multicoil structure designing. For example, a transmitting coil with a tumbler structure is presented in [16] to improve lateral misalignment tolerance; also, [17] proposes a three-dimensional omnidirectional underwater wireless power transfer system to compensate angle misalignment.

On the other hand, some work on circuit resonance compensation plays an important role in WPT research such as [18] presenting a position-insensitive WPT based on nonlinear resonant circuits; [19] summarizing classic compensation topologies that realize constant-current or constant-voltage output as well as zero current switching (ZCS) or zero voltage switching (ZVS). It is also worth mentioning that relay resonator can improve WPT efficiency stability too [20]-[22]. While in some cases, to achieve a high-level integration and a smaller power loss with a strong coupling, compensation on Rx can be eliminated [23].

Although there are various kinds of solutions which have been proposed in recent years, most of them are characterized by lack of simplicity and the whole volume of circuits are not compact enough. Thus, it's usually hard to apply them into engineering practice. In this paper, integrated circuit chips XTK-801 and XTK-3170 are adopted to

control operating frequency and series compensation circuits are soldered on two 4 cm *
2 cm PCB boards as Tx and Rx respectively. As a result, the presented WPT system can
work steadily at 24 V input voltage, 36 W output power maximum and stable 12 V output
voltage versus coupling coefficient change in a range from 0.2 to 0.8. The third part
includes coil design and simulation. The fourth is an experimental and discussion part
which is following by conclusions.

2.1.2   WPT Coil Structures

As shown in previous section, the dimension, shape and structure of the coils have a
great influence on WPT efficiency especially when angle between the coil planes are
different by "0" or the coils' axis misalignment appear. Conventional coil structures used
in WPT such as planar spiral coil or cylindrical spiral coil have good simplicity in design,
but they are very sensitive to misalignment and distance change. To solve this, some
researchers put magnetically permeable medium in the center of the coil to concentrat
magnetic flux, while some others just work with coil shape arrangement like double-D
coils or simply adopt multi-transmission coils [24]. Figure 2 shows 4 common coil
structures where (a) is planar spiral coils with double layers, (b) is planar coils with ferrite
core, (c) is triple coils structure and (d) is double-D coil structure.

(a)   (b)

(c)   (d)
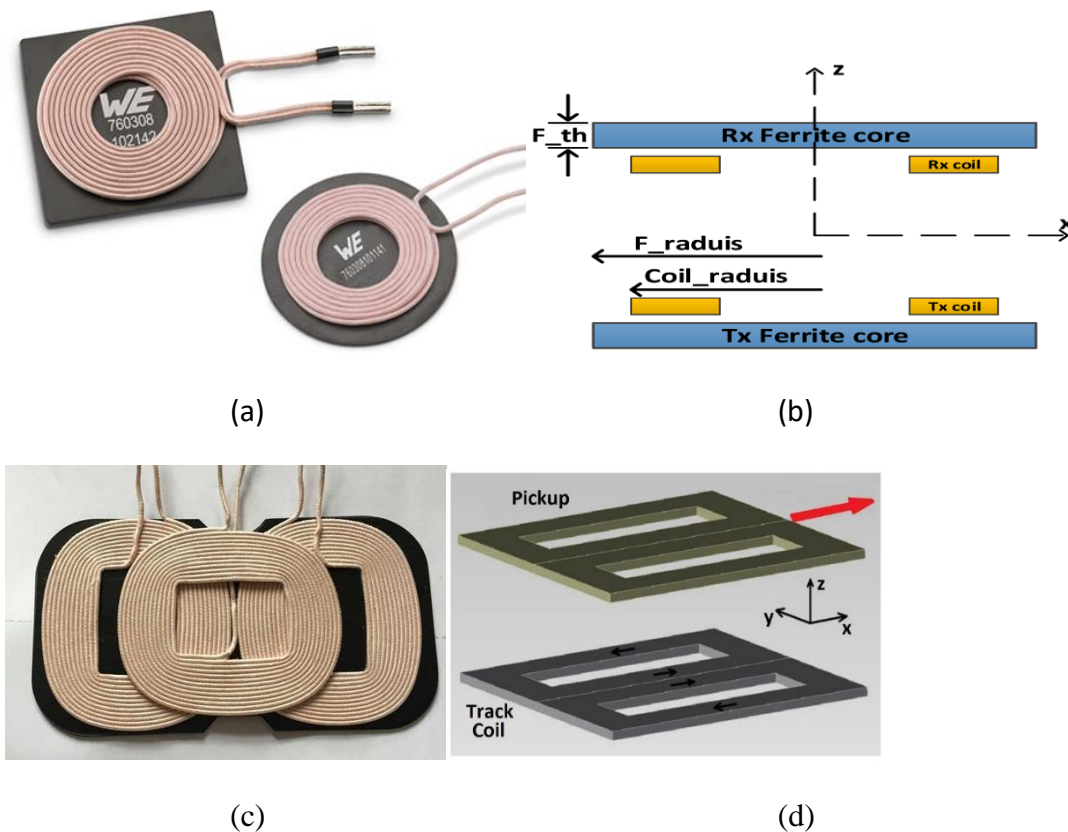
Figure 2 —WPT coil structures

2.1.3   WPT applied in water environment

Recently, as the world put more and more emphasis on the marine resource development, wireless power transfer underwater has attracted attention and been applied rapidly, such as autonomous underwater vehicle (AUV) and unmanned surface vehicle (USV). However, power supply is the main factor which limits the equipment from long-time operation. Based on wireless power transfer underwater (WPTU), the tightness, flexibility and practicality can be significantly improved by using WPTU charging base station. In [25], it introduces an underwater observation laboratory located on the seabed. The system has several sensors providing real-time captures and including a camera and temperature, salinity, conductivity and pressure sensors. Clearly, WPTU is capable of power supply for such kind of underwater devices.
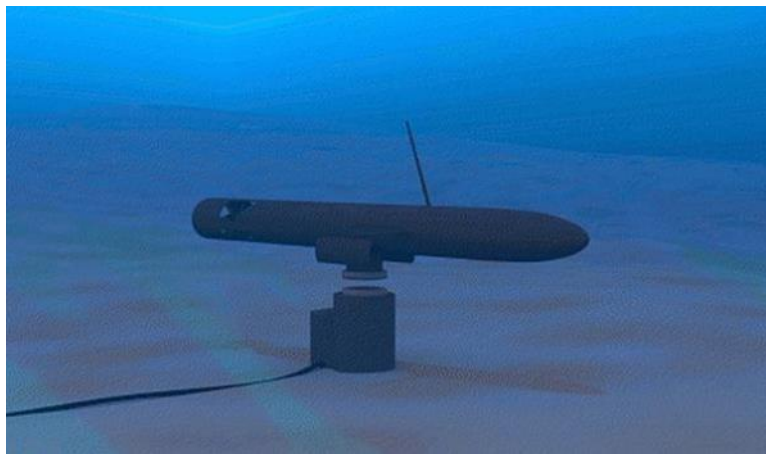
Figure 3 一WPTU charging station for AUV

2.1.3.1.   Global research status on WPTU

Different from WPT in the air, the transmission efficiency of WPTU usually decreases as the conductivity, permeability and permittivity in natural water, which cause eddy current loss, is bigger than those in the air. In response to this phenomenon, some papers present experimental analysis, but still lack quantitative theoretical analysis. Thus, in [26], is reported that the phenomenon of frequency splitting disappears at the resonant frequency in hundreds of kHz range, but there's no further theoretical explanation. However, some papers such as [27] and [28] propose theoretical calculation for eddy current loss in WPTU by electromagnetic theory, while [29] does the calculation by adopting circuit model and equating the effect of eddy current to resistance, thereby simplify the calculation process.

Considering the different properties between natural water and air, e.g. the density and buoyancy, it's still worth exploring new ways to improve the efficiency of WPTU.

2.2.   Unmanned surface vehicle

In order to cater the needs of frequent water or underwater detection as well as search and rescue job, techniques relating with unmanned surface vehicles (USVs) have been rapidly developed in recent years. Compared with conventional vehicles, USVs have the following benefits: 1) USVs elimimate the possibility of casualties since there is no personel on crew on board and cost less on maintenance; 2) the lower weight and more compact dimensions help improve the flexibility and save energy; 3) USVs can perform longer and more complex mission.

For such large large advantages over MVs, there are increasing number of researches on USVs. Thus can be mentioned the algal bloom removal robotic system (ARROS) which is designed with a catamaran-type USV assisted unmanned aerial vehicle is presented in [30]; In [31], it proposes heading control of USV with variable output constraint model-free adaptive control algorithm which enhance the robustness of moving; while [30] presents an adaptive null-space-based behavioral (NSB) method to improve adaptability of multiple unmanned surface vehicles (MUSVs) control. And the papers mentioned above mainly focus on navigation and motion control algorithm.

There are a few innovations on energy power of USV reported in the literature. Thus, in [32] it presented the design a fuel-cell-powered catamaran-type unmanned surface vehicle. The solution still cannot solve the problems of high cost and risk of hydrogen production and storage. As a result, it is a promising orientation to apply WPT technology into USV to enhance the working flexibility effevtively. Figure 4 illustrates four fields where USVs are usually applied, military, search and rescue, resource exploration and water surface cleaning.
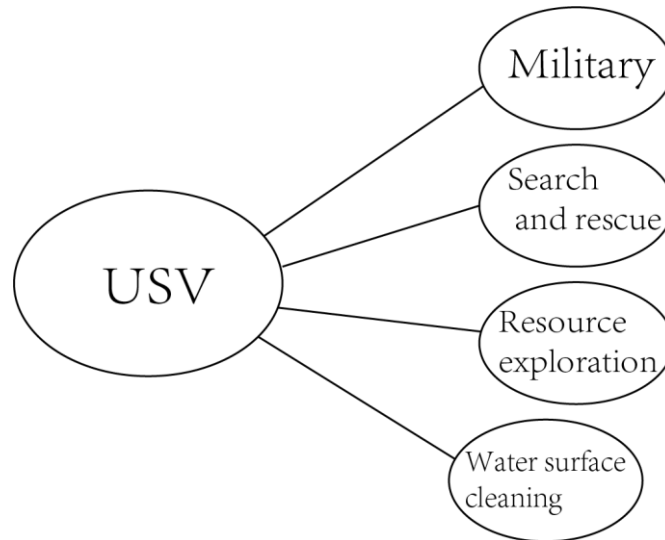
Figure 4 －USV application field

2.2.1.　Common obstacle avoidance (OA) method and path planning for USVs

In practical application scenario, it is common to see some obstacles on water surface such as bridge piers, beacons, rocks or other vessels, thus, the obstacle avoidance which comes with path planning becomes an indispensable function to a full-automatical USVs. As obstacles can be divided in to stationary and moving obstacles, USV needs different kinds of algrithms. For the stationary obstacles, the A* search algorithm [33], which uses a cost analysis and can find an optimal solution in a short time, is a common one. Furthermore, this cost analysis can be extended for other costs like shipping lanes, direction, route time, etc. On the other hand, velocity obstacle is the most intuitive algrithm to avoid moving obstacles since it only needs the relative velocity between the USV and obstacle [34].

In order to make the algorithm implementation, various kinds of sensors are required to be utilized convergently including radar, initial measurement, LIDAR, camera, GPS and sonars at different positions of a hull, such as bow, stern and starboard. Considering a mini USVs, one of the most common distance sensors is ultrasonic ranging moudule which was also utilized in this case. However, for large USVs, a two-tiered obstacle avoidance approach is adopted which consists of a near-field OA component and a far-field OA component which operate in conjunction with each other or simultaneously. Essentially, far-field OA is deliberative path planning which contains automatic identification system (AIS) contact, nautical charts, while near-field OA is reactive avoidance which requires a variety of distance sensors. Figure 5 presnets the tree diagram of USV OA function which can be divided into far-field OA and near-field OA.
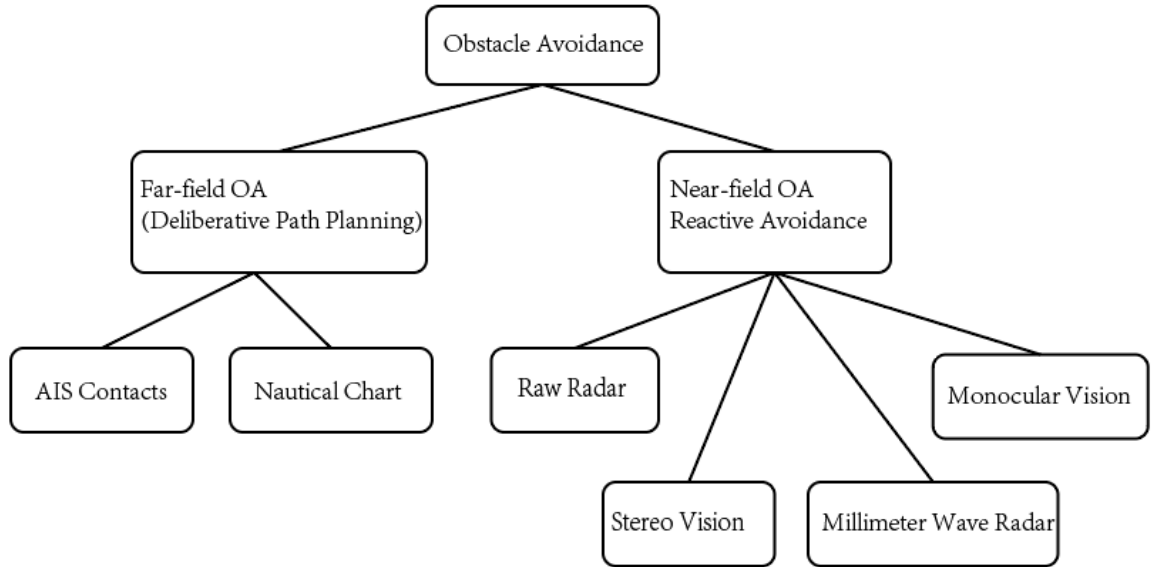
Figure 5 －Large USV OA structure

2.2.2.　Propulsion and power system for USV

Nowadays, there are mainly two propulsion and heading methods. One is provided by rudder and propeller while the other is controlled by differential thrust which is provided by two independent motors. However, these USVs are usually not equipped side actuators or propellers, which means they can be considered as under-actuated USVs, while underactuation is a technical term used in robotics and control theory to describe mechanical systems that cannot be commanded to follow arbitrary trajectories in configuration space [35]. Namely, the degrees of freedom (DOF) in motion of the USV is more than the quantity available actuators and those fully-actuated USVs are relatively simpler to control than the under-actuated ones. Figure 6 (a) and (b) show the illustration of two kinds of propulsion which are single propeller with rudder and differential thrust respectively.

<div align="center">(a)   (b)</div>
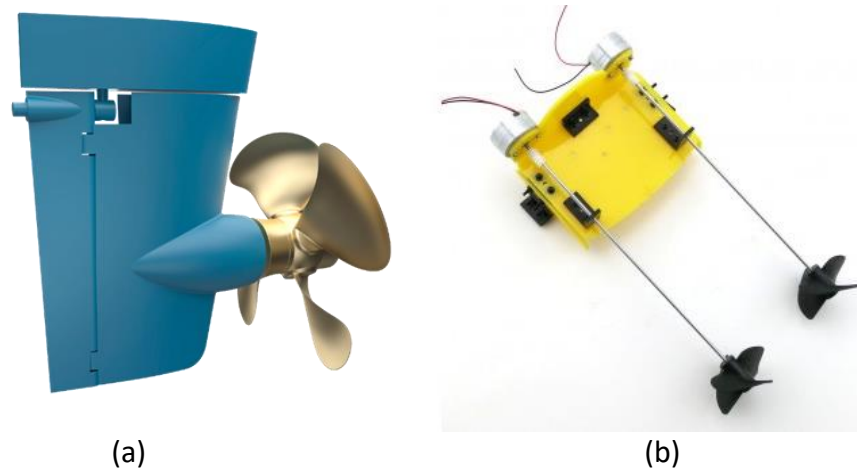
Figure 6 －(a) Propulssion with rudder and propeller; (b) Propulssion by differential thrust.

2.3. Data Transmission with and without Wireless Communication Protocol

In order to transfer data from USV to host PC as well as receive command from the PC, Wireless communication protocols ought to be chosen cautiously considering that the operation distance is usually dependent on the area of water. Moreover, if the USV is out of the range of wireless communication, it will be in great danger. Table 1 shows the comparison among three wireless communication protocols of Wi-Fi, ZigBee and Long Range Radio (LoRa).

Table 1 – Main Wireless communication protocols characteristics [36]

Feature	Wi-Fi	ZigBee	LoRa
IEEE standard	IEEE 802.11	IEEE 802.15.4	IEEE 802.15.4g
Max Signal Rate	54 Mbps	250 kbps	2-19 Mbps
Range	250 m	10-100 m	1000 m
Frequency	900MHz, 2.4GHz, 3.6GHz, etc.	2.4GHz	431 MHz to 478 MHz
Nodes	Unlimited (ad hoc);2007(infrastructure)	>65000	9
Typical Power Consumption	100-350 mA	1-10 mA	28 mA
Complexity	High	Low	Low

2.3.1.　IEEE 802.11－Wi-Fi

Wireless Fidelity (Wi-Fi) includes the IEEE 802.11 standard, providing a wireless connection todevices within a Wireless Local Area Network (WLAN). Wi-Fi essentially uses an infrastructure network, which also supports sd-hoc networks in infrastructure mode. It allows users to browse the internet at broadband speeds when connected to an access point or are in ad-hoc mod [37], it allows fast data transmission and can handle large amounts of data.

However, the Wi-Fi range depends on the version of Wi-Fi which the device is running. Usually, the latest version has more range than any older ones, e.g. the maximum linkrate of Wi-Fi 6E with 6GHz adopted in 2019 is 600 to 9608 Mbit/s which is much higher than Wi-Fi 5 2014 with 433 to 6933 Mbit/s linkrate and 5GHz frequency. Moreover, physical obstacles in open spaces will have more range than indoors with walls or other interfering objects [38]. In Table 2, it presents the advantages and disadvantages of the Wi-Fi protocol.

Table 2 – Advantages and disadvantages of the Wi-Fi protocol

Advantages	Disadvantages
Decent coverage, outreach and can penetrate walls and other obstacles on the way	High energy consumption
Adding or removing devices from a Wi-Fi network is simple	Radio waves in the network may interfere with other equipment

2.3.2.　IEEE 802.15.4－ ZigBee

ZigBee over IEEE 802.15.4 standard is a technology which sets specifications for WPAN to support low power devices. This communication protocol provides self-organized, multi-hop and reliable networks with long battery life [39].

There are two types of devices which participate in ZigBee networks: Full Function Device (FFD) and Reduced Function Device (RFD). An FFD is able to communicate with RFDs and other FFDs but one RFD can only communicate with one FFD. The FFD can operate in three modes: as a network coordinator, a router and end-node. There is only one coordinator in the ZigBee network, which controls the network, delegates the functions devices of the network, stores the security keys and makes bridges to other

networks. The router works as an intermegiary or to transmit data within the network. The end-node cannot communicate directly with others, it can only talk to the parent nodes, namely the coordinator or router. These devices are designed to spend most of the time in suspension and wake up to transfer data to the parent nodes. This type of network can have multiple end-nodes. In Table 3, it presents the advantages and disadvantages of the ZigBee protocol.

Table 3 – Advantages and disadvantages of the ZigBee protocol

Advantages	Disadvantages
- Low power consumption - Support star, tree and P2P topologies - Supports lots of slaves - One coordinator can control lots of slaves	-Requires additional equipment -Is incompatible with other network protocols

2.3.3. IEEE 802.15.4g — LoRa

Long Range (LoRa) is a low-power and wide-area network (LPWAN) protocol developed by Semtech. It is based on spread spectrum modulation techniques derived from chrip spread spectrum (CSS) technology. It uses license-free sub-gigahertz radio frequency bandslike 433 MHz. LoRa enables long-range transmissions (more than 10 km in rural area) with low power consumption. The technology covers the physical layer, while other technologies and protocols such as LoRaWAN (Long Range Wide Area Network) cover the upper layers. It can achieve data from 27 Kbps to 0.3 Kbps depending upon the spreading factor.

A radio-frequency (RF) module is usually a small electronic device used to transmit and/or receive radio signals between two devices. In an embedded system it is often desirable to communicate with other devices wirelessly. This wireless communication may be accomplished through optical or RF communication. For many applications, the medium of choice is RF since it does not require line of sight. RF communications incorporate a transmitter and a reciever. They are of various types and ranges. Some can transmit up to 150 m. RF modules are typically fabricated using RF CMOS technology [40].

Several carrier frequencies are commonly used in commercially available RF modules, including those in the industrial, scientific and medical (ISM) radio bands such as 433.92 MHz, 915 MHz, and 2400 MHz. These frequencies are used because of national and

international regulations governing the used of radio for communication. Short Range Devices may also use frequencies available for unlicensed such as 315 MHz and 868 MHz. In Table 4, it presents the advantages and disadvantages of LoRa protocol.

Table 4 – Advantages and disadvantages of LoRa

Advantages	Disadvantages
- Long transmit distance - Strong anti-interference ability - High sensitivity - Low power consumption - Easy to operate	- Low bandwidth - Doesn't allow continuous sending - Only for short and periodical communications

2.3.4. Remarks

After comparing the advantage and disadvantage among three wireless communication protocol, finally LoRa is preferred. In this case, Wi-Fi is not appropriate because it is designed for long connections and with a high power consumption, which can reduce the authonomy of the USV. On the other hand, considering the data transmission distances in real environment of surface water the ZigBee it is not appropiate too. Thus, the communication between the USV and host PC will be made through APC 220 RF module with LoRa considering the range uo to 1200m.

2.4. Hardware components

The proposed system is based on a microcontroller. The chosen solution is considered after evaluation of different possible solutions according to the system requirements: signal acquisition, moving control, multisensory interface, data storage and data communication. These devices are used to build embedded systems and electronic projects. These are several boards to do this type of projects such as Raspberry Pi or BeagleBone microcomputers, but the most common one is Arduino.

2.4.1. Arduino

Arduino is open-source hardware. The hardware reference designs are distributed under a Creative Commons Attribution Share-Alike 2.5 license and are available on the Arduino website. Layout and production files for some versions of the hardware are also available.

Most Arduino boards consist of an Atmel 8-bit AVR microcontroller (ATmega8, ATmega168, ATmega328, ATmega1280, or ATmega2560) with varying amounts of

flash memory, pins, and features [41]. The 32-bit Arduino Due, based on the Atmel SAM3X8E was introduced in 2012 [42]. The boards use single or double-row pins or female headers that facilitate connections for programming and incorporation into other circuits. These may connect with add-on modules termed shields. Multiple and possibly stacked shields may be individually addressable via an I²C serial bus. Most boards include a 5 V linear regulator and a 16 MHz crystal oscillator or ceramic resonator. Some designs, such as the LilyPad, run at 8 MHz and dispense with the onboard voltage regulator due to specific form-factor restrictions.

Arduino microcontrollers are pre-programmed with a boot loader that simplifies uploading of programs to the on-chip flash memory. The default bootloader of the Arduino Uno is the Optiboot bootloader [43]. Boards are loaded with program code via a serial connection to another computer. Some serial Arduino boards contain a level shifter circuit to convert between RS-232 logic levels and transistor–transistor logic (TTL) level signals. Current Arduino boards are programmed via Universal Serial Bus (USB), implemented using USB-to-serial adapter chips such as the FTDI FT232. Some boards, such as later-model Uno boards, substitute the FTDI chip with a separate AVR chip containing USB-to-serial firmware, which is reprogrammable via its own ICSP header. Other variants, such as the Arduino Mini and the unofficial Boarduino, use a detachable USB-to-serial adapter board or cable, Bluetooth or other methods. Table 5 shows the available Arduino models with their features.

Table 5 – Comparison among different Arduino types [43]

Name	Analog In/Out	Digital IO/PWM	Dimensions	Weight	USB	Price
101	6/0	14/4	68.6 x 53.4 mm	34 g	Y	28.65 €
Lily Pad	6/0	14/6	50 mm	No Info	N	17.95 €
Mega 2560	16/0	54/15	101.52 x 53.3mm	37 g	Y	35 €
Micro	12/0	20/7	48 x 18 mm	13 g	Y	18 €
MKR1000	7/1	8/4	61.5 x 25 mm	32 g	Y	30.99 €
Uno	6/0	14/6	68.6 x 53.4 mm	25 g	Y	20 €
Zero	6/1	14/10	68 x 53 mm	12 g	Y	39 €
Due	12/2	54/12	101.52 x 53.3mm	36 g	Y	34 €

Ethernet	6/0	14/4	68.6 x 53.3 mm	28 g	Y	39.9 €
Leonardo	12/0	20/7	68.6 x 53.3 mm	20 g	Y	18 €
Mega ADK	16/0	54/15	101.52 x 53.3mm	36 g	Y	43 €
Mini	8/0	14/6	30 x 18 mm	No Info	N	14 €
Fio	8/0	14/6	28 x 65 mm	9 g	N	21 €
Nano	8/0	14/6	18 x 45 mm	7 g	Y	20 €

Here we chose Arduino Mega 2560 as the platform on the USV which requires multiple sensors and motors because Mega can provide more PWM outputs, digital and analog I/O than Arduino Uno. On the other hand, Uno is adopted on the charging station, which is used as the platform on the charging station used with range sensor to measure the distance between two coils.

2.5. Lithium Polymer (LiPo) Battery and its Charging

As the power source of the USV, the battery has to be chosen elaborately considering its durability, volume, weight and output power. However, LiPo battery is the best choice because it provides higher specific energy than other lithium battery types and is used in applications where weight is a critical feature, such as mobile devices and radio-controlled aircraft [44].

2.5.1. Charging for LiPo Battery

In general, the standard voltage of one single Lipo battery cell is 3.7 V, which means that in order to gain a higher output voltage, the battery needs to be connected in series. E.g. a LiPo battery whose standard voltage is 11.1 V is composed of 3 cells in series. While this kind of battery can provide higher power in a simple way, it also brings some problems in charging. Because the internal resistance of every cell may have a little difference from each other, the state of charge for the cells may not be able to keep the same. As a result, if the battery is not charged properly, one of the cells will be overcharged, which can damage the battery and shorten its service life. To solve this problem, a balance charger needs to be use when charging those LiPo batteries. Figure 8 shows the development of the batteries that since Lithium battery was first commercially available in 1992, it has been developing for decades, but still lacks revolutional breakthrough on energy density. However, compared with other batteries like acid or

16

nickel batteries on weight and energy density, lithium batteries are the best option for USVs.
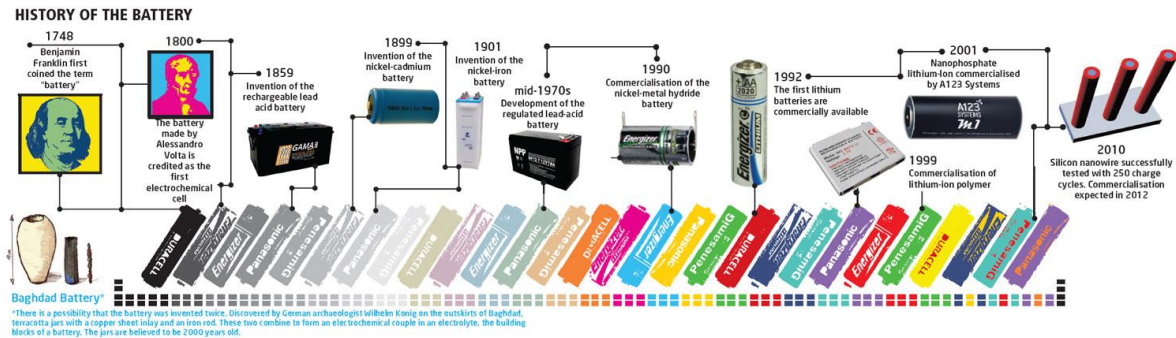
Figure 8 —Development of lithium batteries

2.5.1.1. Battery Balancing

Battery balancing and battery redistribution refer to techniques that improve the available capacity of a battery pack with multiple cells (usually in series) and increase each cell's longevity [45]. A battery balancer or battery regulator is an electrical device in a battery pack that performs battery balancing. Balancers are often found in lithium-ion battery packs for laptop computers, electrical vehicles. etc.

Balancing can be active or passive [46]. The term battery regulator typically refers only to devices that perform passive balancing. In passive balancing, energy is drawn from the most charged cell and dissipated as heat, usually through resistors. In active balancing, energy is drawn from the most charged cell and transferred to the least charged cells, usually through capacitor-based, inductor-based or DC-DC converters. Figure 9 shows a common balance charging circuit diagram which includes a microcontroller, Lipoly battery, three MOSFET transistors and diods.
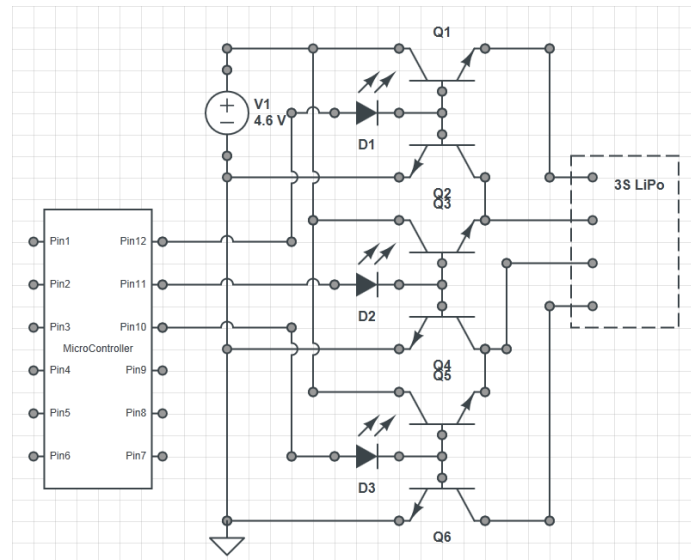
Figure 9 －Banlance charging circuit

2.5.1.2. Constant Current / Constant Voltage (CCCV) Charging

Constant current / constant voltage (CCCV) is a combination of the above constant current and constant voltage charge method. The charger limits the amount of current to a pre-set level until the battery reaches a pre-set voltage level. The current then reduces as the battery becomes fully charged. The lead lithium battery generally uses the CCCV charge method because of its safety and fast charging rate [47]. Figure 10 illustrates the CC/CV charging curve for lithium battery charging.
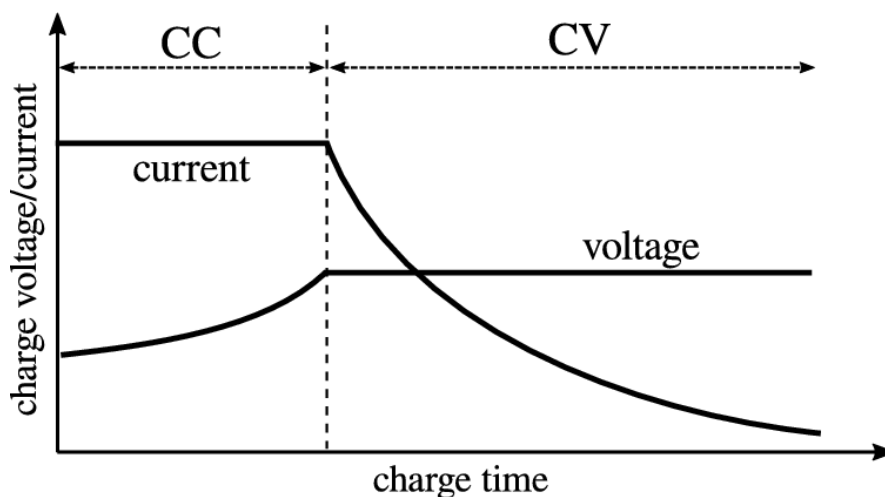
Figure 10 － CCCV charging curve

2.6. Host PC Software

Nowadays, there are a lot of programe development environment such as C, C++, BASIC, JAVA and Python. However, these computer languages all produce codes based on text and lack intuitiveness which is important to engineering application. Different from the environment mentioned above, LabVIEW uses graphic editting language G to program in block diagram which is more suitable for industry process and instrumentation interface. Figure 11 shows three main application fields of LabVIEW including test and measurement, simulation and control system.
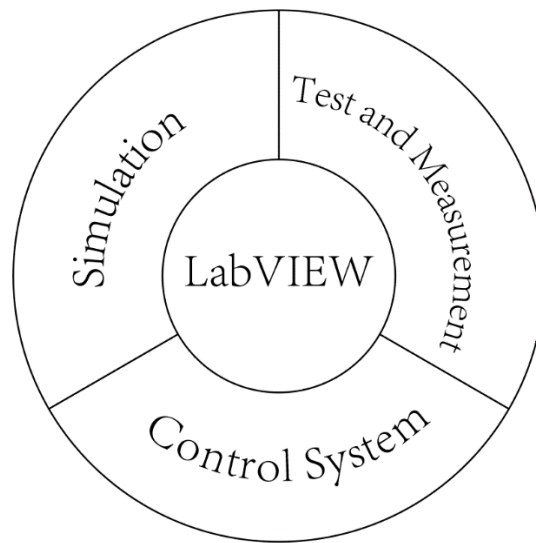
Figure 11 －Applications of LABVIEW

2.6.1. Dataflow Programming

The programming paradigm used in LabVIEW, sometimes called G, is based on data availability [48]. If there is enough data available to a subVI or function, that subVI or function will execute. Execution flow is determined by the structure of a graphical block diagram (the LabVIEW-source code) on which the programmer connects different function-nodes by drawing wires. These wires propagate variables and any node can execute as soon as all its input data become available. Since this might be the case for multiple nodes simultaneously, LabVIEW can execute inherently in parallel [49]:1–2 Multi-processing and multi-threading hardware is exploited automatically by the built-in scheduler, which multiplexes multiple OS threads over the nodes ready for execution.

2.6.2. Graphical Programming

LabVIEW integrates the creation of user interfaces (termed front panels) into the development cycle [50]. LabVIEW programs-subroutines are termed virtual instruments (VIs). Each VI has three components: a block diagram, a front panel, and a connector pane. The last is used to represent the VI in the block diagrams of other, calling VIs. The front panel is built using controls and indicators. Controls are inputs: they allow a user to supply information to the VI. Indicators are outputs: they indicate, or display, the results based on the inputs given to the VI. The back panel, which is a block diagram, contains the graphical source code. All of the objects placed on the front panel will appear on the back panel as terminals. The back panel also contains structures and functions which perform operations on controls and supply data to indicators. The structures and functions are found on the Functions palette and can be placed on the back panel. Collectively controls, indicators, structures, and functions are referred to as nodes. Nodes are connected to one another using wires, e.g., two controls and an indicator can be wired to the addition function so that the indicator displays the sum of the two controls. Thus, a virtual instrument can be run as either a program, with the front panel serving as a user interface, or, when dropped as a node onto the block diagram, the front panel defines the inputs and outputs for the node through the connector pane. This implies each VI can be easily tested before being embedded as a subroutine into a larger program.

The graphical approach also allows nonprogrammers to build programs by dragging and dropping virtual representations of lab equipment with which they are already familiar. The LabVIEW programming environment, with the included examples and documentation, makes it simple to create small applications. This is a benefit on one side, but there is also a certain danger of underestimating the expertise needed for high-quality G programming. For complex algorithms or large-scale code, it is important that a programmer possess an extensive knowledge of the special LabVIEW syntax and the topology of its memory management. The most advanced LabVIEW development systems offer the ability to build stand-alone applications. E.g., the LabVIEW Real-Time Module is a software add-on for LabVIEW that can be used to create and deploy real-time, distributed system applications for test, monitoring, and control. Take advantage of a Real-Time OS to ensure reliability and precise timing in stand-alone system. Furthermore, it is possible to create distributed applications, which communicate by a

client–server model, and are thus easier to implement due to the inherently parallel nature of G [51].

Chapter 3 – System Description

3.1. Overview

This work focusses on the USV development, which can be charged with inductive WPT system in order to improve convenience and safety of charging since the conventional charging system requires plugging connectors frequently, which may cause damage in environment with high humidity. Meanwhile, the USV motion can be controlled remotely or can present autonomous control and the data of battery voltage will be sent to host PC in real time. Figure 12 illustrates the whole system architecture which is divided into three parts.
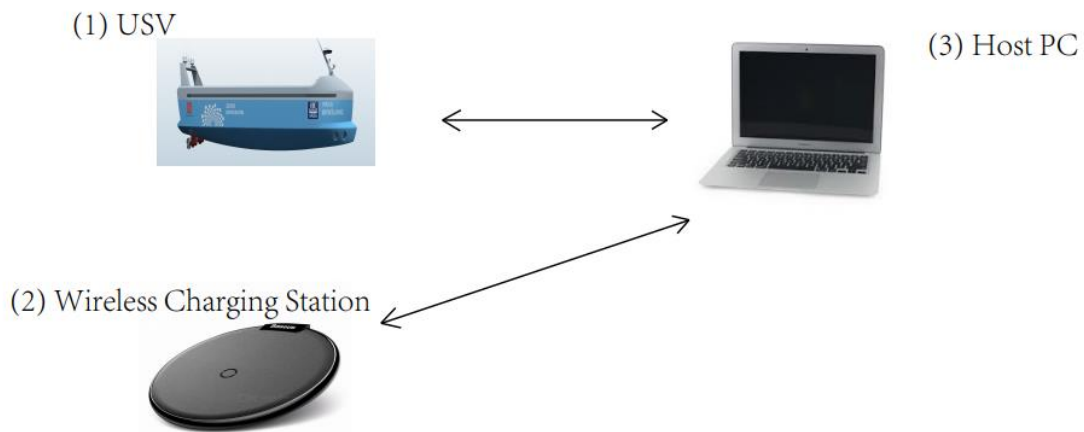
Figure 12 – System Architechture

Basically, the first part (1) the main body of the USV is dedicated to transfer data and perform tasks while the main purpose in this work is to charging it wirelessly. The second part (2) is the wireless charging station which is responsible to charge the USV battery, maintaining the coils aligned well and near each other in order to keep the highest transmission efficiency while protect the Rx circuit. The last part (3) is the host PC which is dedicated to reveive the data and give the control instruction. The software is programmed by LabView.

3.2. Main Hardware Components

3.2.1   Arduino Mega 2560

The Arduino Mega [52] works as the controller of the USV. It is a computation platform which can reveive data from the sensors. The Arduino platform presents PWM signals output which are changed according to the distance between the hull and obstacle,

to the Electric Speed Control (ESC) to regulate the rotation rate of the DC brushless motors.

This Arduino is based on the ATmega 2560 and it is chosen for the USV controller because of the large mount of pins which means more sensors can be used into the system compared with other Arduino boards, as seen in section 2.4.1. Most importantly, it has 12 PWM outputs, 5 pairs of communication ports, 16 Analog In and 28 Digital MISO that enable it to control multiple motors, sensors and communication modules.
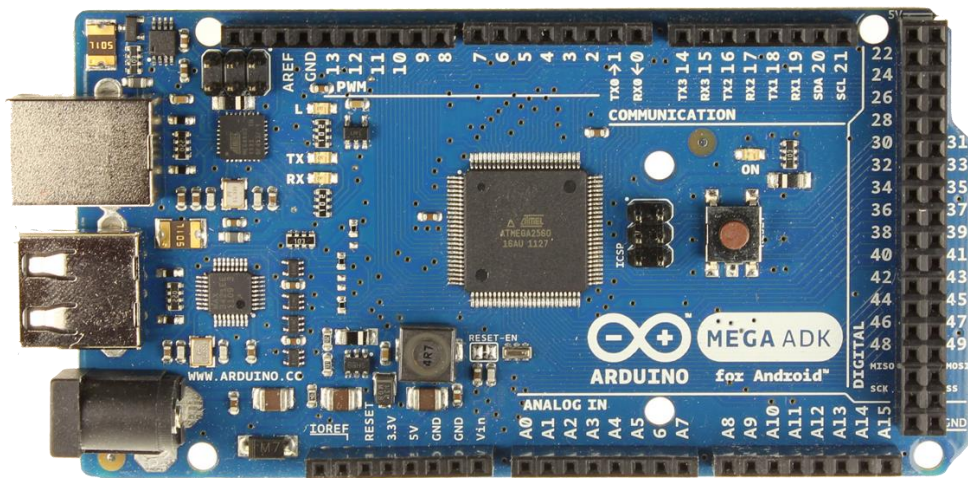
Figure 13 – Arduino Mega 2560

3.2.2. Arduino Uno

The other microcontroller is used on the charging station working with a HC-rs04 to measure the distance between the platform and water surface in order to get the the coil distance. The Arduino Uno is a microcontroller board based on the ATmega328 (datasheet) [53]. It has 14 digital input/output pins (of which 6 can be used as PWM outputs), 6 analog inputs, a 16 MHz ceramic resonator, a USB connection, a power jack, an ICSP header, and a reset button. It contains everything needed to support the microcontroller; simply connect it to a computer with a USB cable or power it with an AC-to-DC adapter or battery to get started.

Figure 14 – Arduino Uno

3.2.3. DC Brushless Motors and Electric Speed Controls (ESCs)

In this work, two NTM Prop Drive Series 28-30A 750kv motors are chosen due to its stable performance. Since the USV in this case is not designed for high speed running, motors with higher power consuming are not suitable.

The motors adopted are rock-solid performance outrunners with tight windings, quality bearings, correctly rated magnets, balanced stator and flux rings plus they are QC checked at 14 points, from material processing all the way through to final dyno test [54]. The specification of the motor is shown in Table 6.

Table 6 – Specifics of NTM Prop Drive Series 28-30A 750kv motor [54]

Specs	
Model	NTM Prop Drive Series 28-30A 750kv
Kv	750rpm/v
Max Current	20A
Max Power	120W @ 12v (3S) / 140W @ 15v (4S)
Shaft	3mm
Weight	67.1g
ESC	25A
Cell Count	3s-4s Lipoly
Bolt Holes	16mm & 19mm

Bolt thread	M3
Connection	3.5mm Bullet-connector

Figure 15 – NTM Prop Drive Series 28-30A 750kv DC brushless motor

In order to control and regulate the speed of brushless motors, it is necessary to connect two electronic speed control (ESC) modules. ESC may also provide reversing of the motor and dynamic braking. Miniature ESCs are used in electrically powered RC models.

The ESC used in this case is a HW30A Brushless Motor ESC whose input power is 5.6V – 16.8V with 2A battery elimination circuit and constant current is 30A [54]. The ESC is featured by safe power function: regardless of the throttle stick in any position the motor will not start immediately; throttle Calibration function: adapt to different remote throttle travel difference, improve throttle response linearity, with a smooth, delicate feel and excellent speed linear speed; low voltage protection mode and low-voltage protection threshold. The specification of the ESC is shown in Table 7.

Table 7 – Specifics of 30A ESC

Specs	
Output	30A continuous; 40A for 10 seconds
Input voltage	2-4 cells Lithium Polymer / Lithium Ion battery or 5-12 cells NiMH / NiCd
BEC	5V, 3A for externzl receiver and servos

Max Speed	2 Pole: 210,000rpm; 6 Pole: 70,000rpm; 12Pole: 35,000rpm
Weight	32gms
Size	55mm x 26mm x 13mm
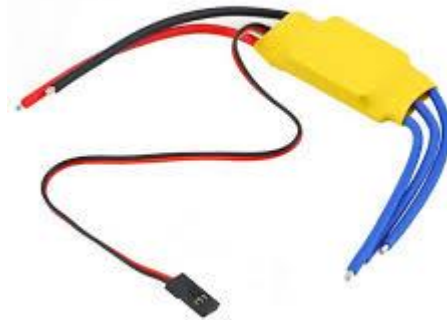
Figure 16 – 30A Electric speed control (ESC)

3.2.4   HC-SR04 Ultrasonic Sensor

To realize obstacle avoidance with low cost and high accuracy, we use HC-SR04 to measure the distance between the hull and obstacle in static state in real time. Ultrasonic ranging module HC - SR04 provides 2cm - 400cm non-contact measurement function, the ranging accuracy can reach to 3mm. The module includes ultrasonic transmitters, receiver and control circuit. The basic principle of ultrasonic sensor is presented in [55]:

(1) Using IO trigger for at least 10us high level signal,

(2) The Module automatically sends eight 40 kHz pulses and detect whether there is a pulse signal back.

(3) IF the signal back, through high level, time of high output IO duration is the time from sending ultrasonic to returning.

Test distance = (high level time×velocity of sound (340M/S) / 2. Table 7 illustrates the electric parameter of the module

Table 7 – Electric Parameter [55]

Specs	
Working Voltage	DC 5V
Working Current	15mA
Working Frequency	40Hz
Max Range	4m
Min Range	2cm
Measure Angle	15 degree
Trigger Input Signal	10uS TTL pulse
Echo Output Signal	Input TTL lever signal and the range in proportion
Dimension	45*20*15mm

Figure 17 – HC-SR04 Ultrasonic Sensor

3.2.5   Micro Servo Motor

In order to measure distance in a wider range in angle (-45 to 45 degrees in this case), a servo motor where the ultrasonic sensor sticks is adopted so that the sensor can spin around with the servo motor. A servomotor is a rotary actuator or linear actuator that allows for precise control of angular or linear position, velocity and acceleration. It consists of a suitable motor coupled to a sensor for position feedback. It also requires a relatively

sophisticated controller, often a dedicated module designed specifically for use with servomotors.

The TowerPro SG90 mini servo is lightweight, high-quality and lightning-fast. The servo is designed to work with almost all the radio control systems [56]. The SG90 mini servo with accessories is perfect for R/C helicopter, plane, car, boat and truck use. Figure 18 shows the servo motor PWM period which is 20 ms (50 Hz) and the duty cycle is 1-2 ms. Table 8 illustrates the specifications of the servo.

Table 8 – Servo Specifications

Specs	
Speed (sec)	0.1
Torque (kg-cm)	2.5
Weight (g)	14.7
Voltage	4.8 - 6
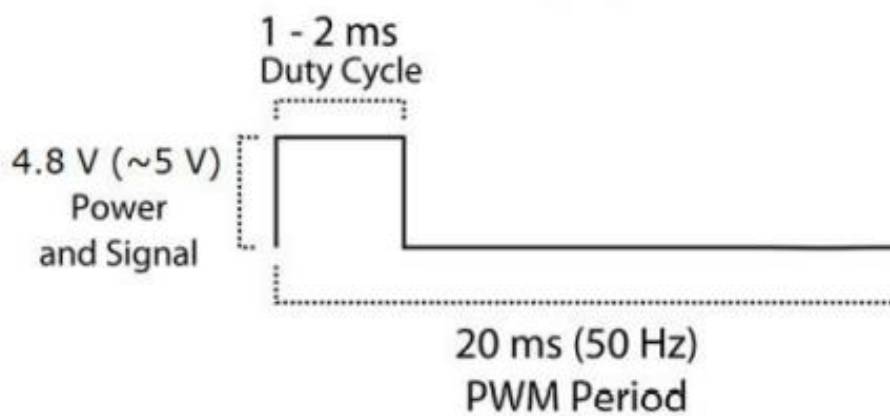
Figure 18 – Servo motor PWM period

Figure 19 – Servo motor

3.2.6 Lipoly Battery

To supply the whole SUV system including the propellers, sensors and controller, ZIPPY 2200mAh 3S 35C Lipo pack which is chosen for its compact size and excellent performance. Compared with other types, it can provide the same capacity and discharge rate while the size and weight are much smaller. The battery specification is shown in Table 9.

Table 9 – Battery Specification [57]

Specs	
Capacity	2200mAh
Voltage	3S1P / 3 Cell / 11.1V
Discharge	25C Constant / 35C Burst
Weight	163g (including wire, plug & case)
Dimensions	107x24x34mm
Balance Plug	JST-XH
Discharge Plug	XT60

Figure 20 – ZIPPY Battery

3.2.7 Funduino Voltage Sensor

In order to measure external voltages greater than 5 V using Arduino, voltage sensor module which can measure voltages up to 25 V is introduced.

Basically, a 25V Voltage Sensor, like the one used here, has 5 pins in total [58]. Two of them are on the two-pin screw terminal and three are male header pins. The Screw Terminal pins are marked as VCC and GND and they must be connected to the external source of voltage i.e. the voltage that needs to be measured. The Voltage Sensor is basically a Voltage Divider consisting of two resistors with resistances of 30KΩ and 7.5KΩ i.e. a 5 to 1 voltage divider. Figure 21 shows the schematic of the Voltage Sensor Module with an input voltage limit of 25V. The specifications of the voltage sensor that we use is shown in Table 10

Table 10 – Voltage Sensor Specifications

Specs	
Input Voltage	0 to 25 V
Voltage Detection Range	0.02445 to 25
Analog Voltage Resolution	0.00489 V
Dimensions	4 x 2 x 3 cm
Advantages	1. Needs no external components 2. Easy to use with microcontrollers 3. Small, cheap and easily avaailable
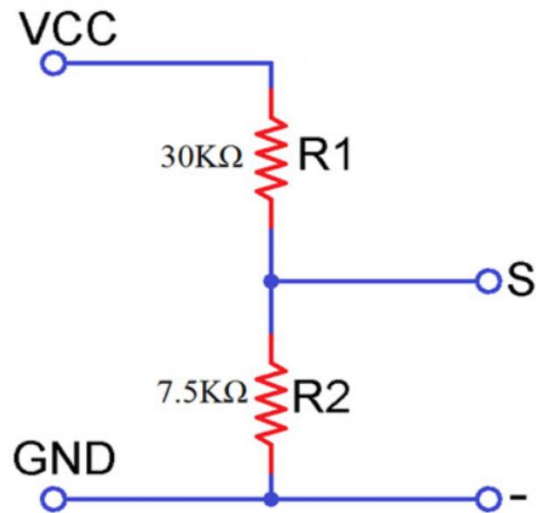
Figure 21 – Funduino Voltage Sensor circuit

Figure 22 – Funduino Voltage Sensor

3.2.8. Wireless Communication Module APC220

APC220 is highly integrated semi-dulex low power transceiver module with high speed MCU and high performance RF IC. Utilizing high efficiency forward error correction with interleaving encoding (FEC) technology, it makes anti-interference ability and reception sensitivity greatly improved. It also can ensure good performance in the hash environment such as in the industrial application. The FEC technology is advanced and unique in radio data communication field.

APC220 is a cost-effective and easy-usable module that not only can transmit transparent data with large data buffer, but also can provide over 100 channels. Users just

need feed data to the module through serial port. The simply-configuration function and compact size make it an ideal option for radio data communication application. Nowadays it has been used in a lot of fields, e.g. Automated Meter Reading (AMR), wireless sensor, industrial automation, wireless handheld terminal and control of traffic signal, etc. Figure is a picture of APC220 module and Table 11 shows APC220 Specifications.

Table 11 – APC220 Specifications

Specs	
RF line-in-sight distance	800m (9600bps)
Max output power	20mW (13dB)
Frequency	418MHz to 455MHz
Number of channels	More than 100
Data buffer	Exceed 256 bytes

Figure 7 －APC220

The whole USV and charging station hardware wiring is illustrated in Figure 23 and Figure 24 respectively.

Figure 23 – Sketch Scheme
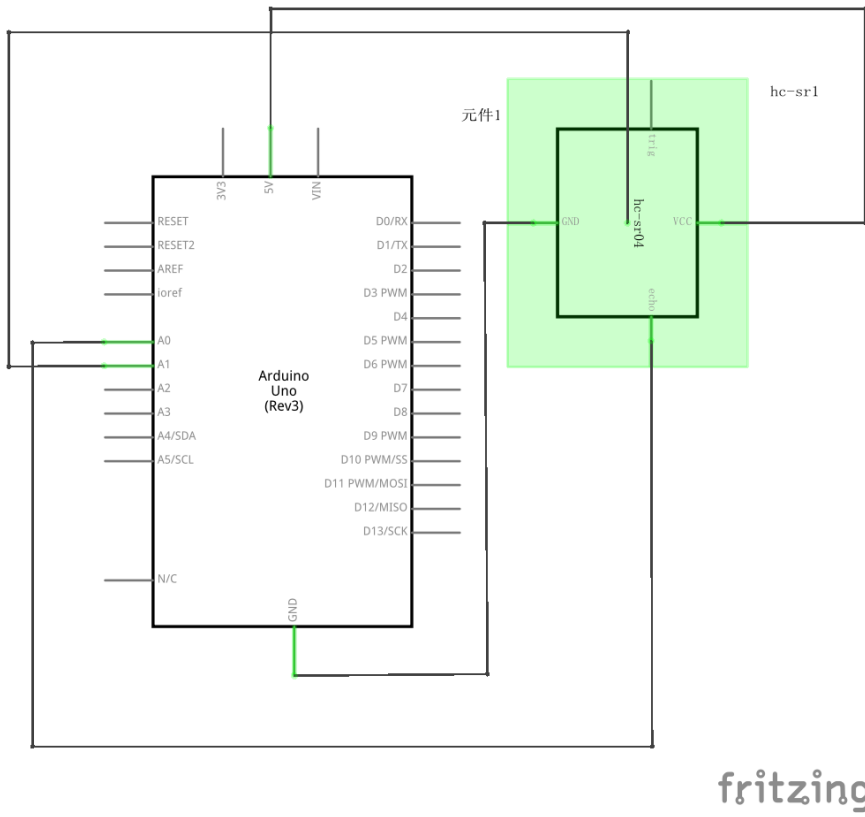
Figure 24 – Power station wiring scheme

Chapter 4 – Methodology

4.1. Design of WPT Charging Station

In order to save the charging time considering the reality that USV needs to be recharged frequently, a WPT charging station which can provide stable voltage out put is designed. In this section, the detail of the WPT charging station will be presented. The structure of the charging station can be divided into two parts which are mechanism and circuit respectively. As the focus of the work, the design of the WPT circuit will be elaborated below firstly.

4.1.1. Design of WPT Circuit for Stable Voltage Output

In this section, the coupling model [59] is considered to analyze components parameters and resonant frequency. The detail of components parameters determination for meeting the output demand is presented as well. In order to calculate more straightly, the whole model is simplified.

4.1.1.1. Circuit Modeling

The WPT circuit structure is composed of transmitting (primary) side and receiving (second) side. In first side, it mainly contains DC power supply, an inverter driven by an integrated frequency generator, resonant compensation circuit and Transmitting coil. In second side, a receiving coil, resonant compensation circuit, rectifier, stabilizer and resistant load are considered. The self-inductances of two coils are L_P and L_S respectively. M represents the mutual inductance.

For convenience of analysis, DC voltage source and inverter can be seen as an AC voltage source. Simultaneously, the load, rectifier and stabilizer can be simplified into a resistant load while two coupling coils can be equivalent to a T-shaped inductance structure after eliminating the mutual inductance as shown in Figure 25. In this paper, series-series (S/S) compensation is utilized considering the necessity to have a constant voltage output and a simple construction.
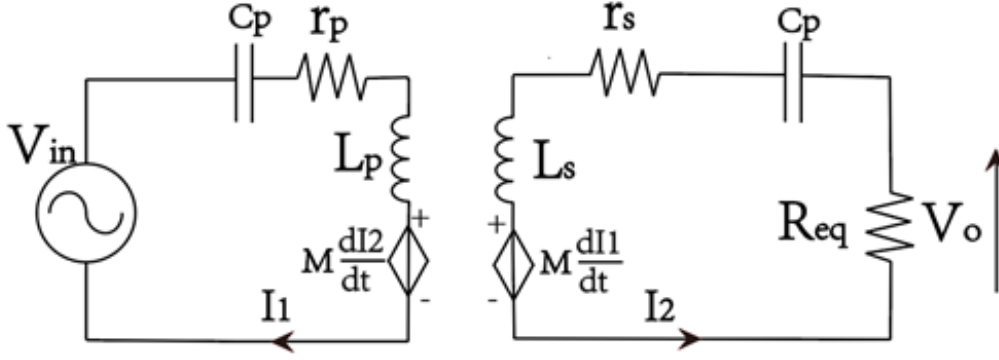
Figure 15 - Simplified WPT circuit with S-S compensation

4.1.1.2. Output Voltage Calculation and Dependances

In an S-S compensation topology as Figure 25, the impedances Z_1 and Z_2 are defined as follows:

$$Z_1 = (L_p\omega - \frac{1}{\omega C_p})j + r_p \tag{1}$$

$$Z_2 = (L_s\omega - \frac{1}{\omega C_s})j + r_s \tag{2}$$

where C_P and C_S are the capacitances matching with L_P and L_s, ω is the operation frequency, r_p and r_s are the internal resistances in Tx and Rx respectively.

According to Kirchhoff's Law, the equation set is expressed as follows:

$$\begin{cases} U_{in} = Z_1 I_1 + j\omega M I_2 \\ U_o = Z_2 I_2 + j\omega M I_1 \\ \quad U_o = I_2 R_L \end{cases} \tag{3}$$

where I_1 and I_2 are the currents through Tx and Rx respectively, U_{in} is the input voltage and R_L is the load resistance in the equivalent circuit.

Then, the relationship between I_1 and I_2, and the output voltage can be expressed as:

$$I_1 = \frac{I_2(R_L - Z_2)}{j\omega M} \tag{4}$$

$$U_o = I_2 R_L = \frac{R_L U_{in} M \omega j}{(R_L - Z_2)Z_1 - M^2\omega^2} \tag{5}$$

where U_o is the output voltage across the load resistance. Substitute (1) and (2) into (5), assuming $C_p = C_s = C$, $r_p = r_s = r$ and $L_p = L_s = L$, which means $Z_1 = Z_2 = Z$, we can get:

$$U_o = j\omega MI_1 - rI_2 - (j\omega L - \frac{j}{\omega C})I_2 \tag{6}$$

Then it can be gained that U_o is unrelated with R_L when $\omega_0 = \frac{1}{\sqrt{C(L-M)}}$, ω_0 is defined as resonant circular frequency. In addition, the output voltage can also be expressed as follows:

$$U_o = j\omega MI_1 - rI_2 \tag{7}$$

In order to observe the effect of the mutual inductance variations on the output voltage, the partial derivation of the output voltage to the M can be expressed as follows:

$$\frac{\partial U_o}{\partial M} = \frac{\partial}{\partial M}(j\omega MI_1 - rI_2) = j\omega I_1 + j\omega M \frac{\partial I_1}{\partial M} - r \frac{\partial I_2}{\partial M} \tag{8}$$

It can be seen that the change rate of U_o depends not only by M, but also by the variations of the current of the WPT primary side.

4.1.1.3. Inverter Circuit

A power inverter is a power electronic device or circuitry that changes direct current to alternationg current. The input voltage, output voltage and frequency, and overall power handling depend on the design of the specific design or circuitry. The inverter does not produce any power; the power is provided by the DC source. A power inverter can be entirely electronic or may be a combination of mechanical effects (such as a rotary apparatus) and electronic circuitry. Static inverters do not use moving parts in the conversion process [60].

Inorder to increase the transmission efficiency of WPT system, the frequency of the inverter has to be high enough and the value usually need to get to at least kHz level. An inverter can produce a square wave, modified sine wave, pulsed sine wave, pulse width modulated wave (PWM) or sine wave depending on circuit design. Common types of inverters produce square waves or quasi-square waves. One measure of the purity of a sine wave is the total harmonic distortion (THD). A 50% duty cycle square wave is equivalent to a sine wave with 48% THD. Technical standards for commercial power distribution grids require less than 3% THD in the wave shape at the customer's point of connection. IEEE Standard 519 recommends less than 5% THD for systems connecting to a power grid [61].

There are two basic designs for producing household plug-in voltage from a lower-voltage DC source, the first of which uses a switching boost converter to produce a

higher-voltage DC and then converts to AC. The second method converts DC to AC at battery level and uses a line-frequency transformer to create the output voltage.

4.1.1.5. AC-DC and DC-DC Converter Design

4.1.1.5.1. Full Wave Rectifier (AC-DC Converter)

The circuits which convert alternating current (AC) into direct current (DC) are known as rectifiers. If such rectifiers rectify both the positive and negative half cycles of an input alternating waveform, the rectifiers are referred as full wave rectifiers. Alternatively, a rectifier is a device that converts alternating current (AC) to direct current (DC). It does it by using a diode or a group of diodes. We know that a diode permits current only in one direction and blocks the current in the other. We use this principle to construct various rectifiers [62].

Rectifiers can be usually classified into two types that one is half wave rectifier and the other is full wave rectifier. When a half-wave rectifier is used, a significant amount of power gets wasted as the only a half of each cycle passes through and the other is blocked. Moreover, the half-wave rectifier has only around 40.6% efficiency and it cannot be used for applications which require a smooth and steady DC output. For more efficient and steadier DC output, a full wave rectifier is considered. Figure 26 illustrates a typical full-wave bridge rectifier which contains four diods. In this case, a full wave rectifier is set between Rx coil and DC-DC converter to turn AC into DC.
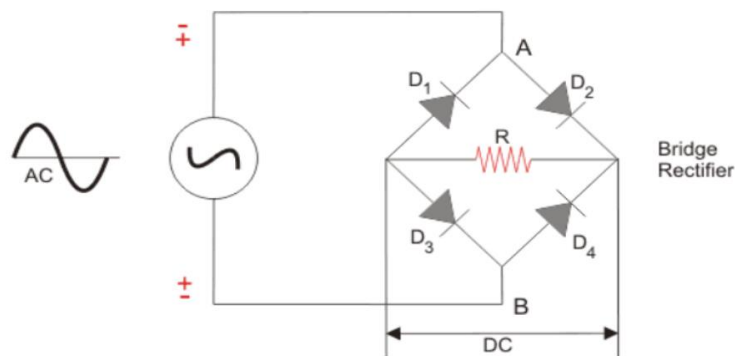
Figure 26-A typical full-wave rectifier

4.1.1.5.2. Buck DC-DC Converter

A buck converter (step-down converter) is a DC-to-DC power converter which steps down voltage (while stepping up current) from its input (supply) to its output (load) [63]. It is a class of switched-mode power supply (SMPS) typically containing at least two

semiconductors (a diode and a transistor, although modern buck converters frequently replace the diode with a second transistor used for synchronous rectification) and at least one energy storage element, a capacitor, inductor, or the two in combination. To reduce voltage ripple, filters made of capacitors (sometimes in combination with inductors) are normally added to such a converter's output (load-side filter) and input (supply-side filter). Figure 27 illustrates a typical buck DC-DC converter. In this case, the buck inductance and stabilizing capacity are set as $33\mu H$ and $220\mu F$ respectively.
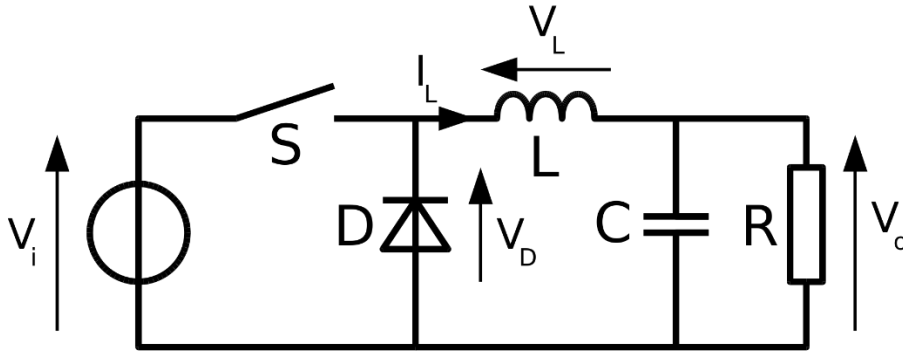
Figure 37-A typical buck DC-DC converter

In order to convert AC voltage from receive side (Rx), an AC-DC converter is designed taking into account the following requirements. Usually, the output voltage in a WPT system is characterized by variations because the mutual inductance decreases when misalignment increasing. For small variations of M, the sensitivity S can be expressed as follows:

$$S = \frac{\partial U_o(P_{out}, M)}{\partial M} \tag{9}$$

where P_{out} is the output power. The sensitivity S above can be used to optimize the stability of output voltage. Furthermore, the efficiency is another key performance index whose constraint can be expressed as follows:

$$\eta = \frac{P_{out}}{P_{in}} \geq \eta_{di} \tag{10}$$

where η and η_{di} are the efficiency and design efficiency, P_{in} is the input power.

According to (12), desired voltage gain, thermal limits, switching and capacitor losses ought to be taken into account because these are the main factors influencing transmission efficiency. Furthermore, in order to stabilize the output voltage, a buck DC-DC converter

39

is considered. In this case, a 36 W/ 85 kHz WPT system of which desired voltage gain is 0.5 and desired efficiency in an operation range is considered to be higher than 80%.

4.1.1.4. Charging Circuit Designs for Balance

There are mainly two plans to achieve battery balance. One is simple that a buck DC-DC converter is connected to WPT output to reduce voltage to 5 V, then a switch circuit with voltage sensor follows behind. This charging circuit charges only one cell at a time. Once it is detected that the cell is fully charged, it will instantly switch to the next until three cells are all fully charged.

The other plan is to charge three cells with 12.6 V simultaneously and voltage of every cell is detected. Once a cell is over charged (> 4.2 V), it will be switched to connect with a resistance to consume extra energy until three cells are all get to 4.2 V in order to protect the battery pack from over charging of single cell. Then charging is off.

Comparing the two designs, it can be found that the first plan takes more time to fully charge the battery while it has higher power transmission efficiency than the second one because it does not need to consume more energy in heat loss. However, in this case time cost is put on more emphasis, so the second balance charging plan which charges all the cells synchronously is chosen.

4.1.2. Coil Design and Simulation

To optimize the WPT system design, simulation of system coils is considered so that the coupling coefficient between Tx and Rx can be maximum. Further, we can obtain the condition of magnetic field when current flows through the coils via simulation.

In this work, planar spiral structure without magnetically permeable medium is considered because of its simplicity and smaller volume in plane compared with other structures like hemispherical and columnar spiral ones. Specifically, the inner and outer diameters of both coils are 30mm and 82 mm respectively with 15 turns winding. Besides, the diameter of the cable used to wind the coils is 1 mm. Figure 28 is the picture of the single-layer planar spiral coil in this case.
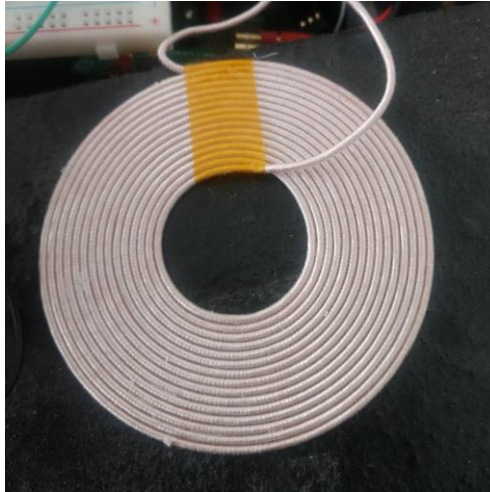
Figure 48- Coil

The effect of coil coupling, the magnetic field situation between two coils was studied by simulation using Ansys Maxwell. Thus, 10 A current is set through the Tx and the result of simulation with and without misalignment is presented in Figure 29. In addition, a Maxwell-Simplorer cosimulation is done under 200 kHz power source with S-S compensation to see the magnetic field change between two coils. In Figure 30, it shows the largest and smallest animation magnetic field produced by Rx coil in one period which indicates that the root mean square (RMS) value of the current in Rx coil is much lower than that in Tx coil, even in resonance. The magnetic field produced by Rx coil changes periodically because the induced current varies in period as the current in Tx coil does. Thus, the magnetic field intensity has a lowest and highest value in one period. Furthermore, Figure 31 (a) and (b) show the coupling coefficient change versus coil distance in range from 5 to 70 mm and misalignment in range of 0 to 40 mm respectively, which indicate that both distance and misalignment influence on coupling coefficient. Especially, it is also noticeable that the attenuation rate of the coupling coefficient versus coil distance is much bigger than that versus misalignment. In another word, the coupling coefficient is more sensitive to the distance change, so it's important to take it into consideration when designing WPT systems.
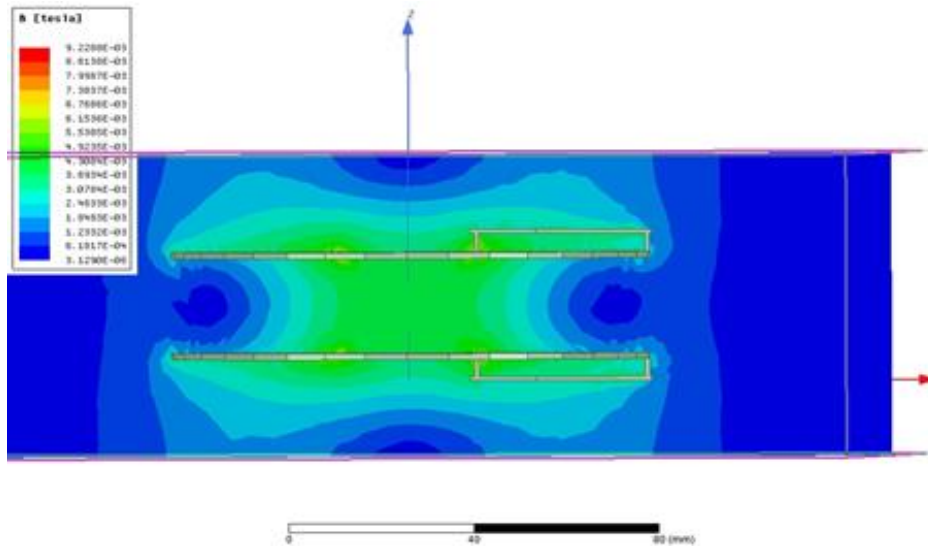
(a)
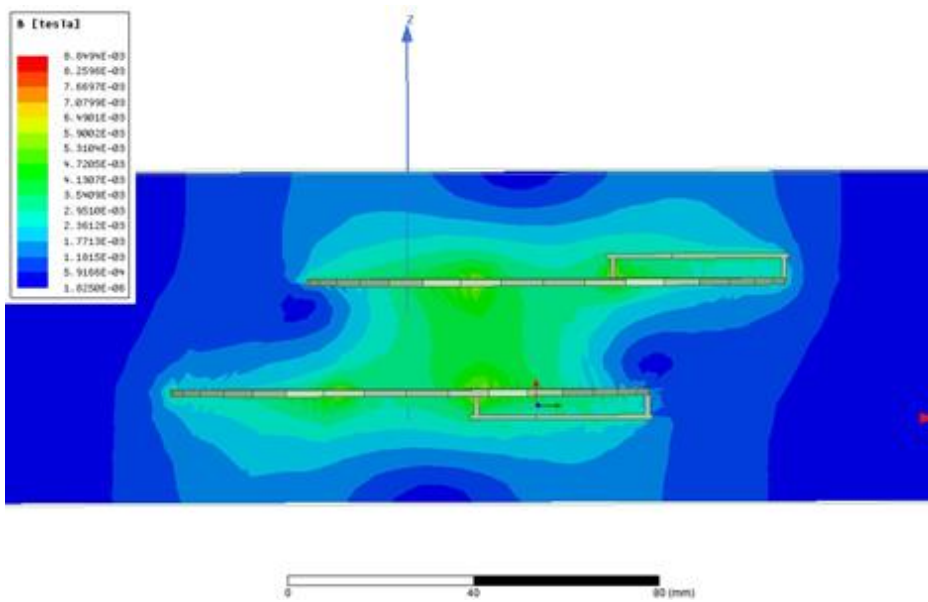
(b)

Figure 29- Magnetic field distribution. (a) Magnetic field distribution for coils without misalignment; (b) Magentic field distribution of the coil with misalignment.
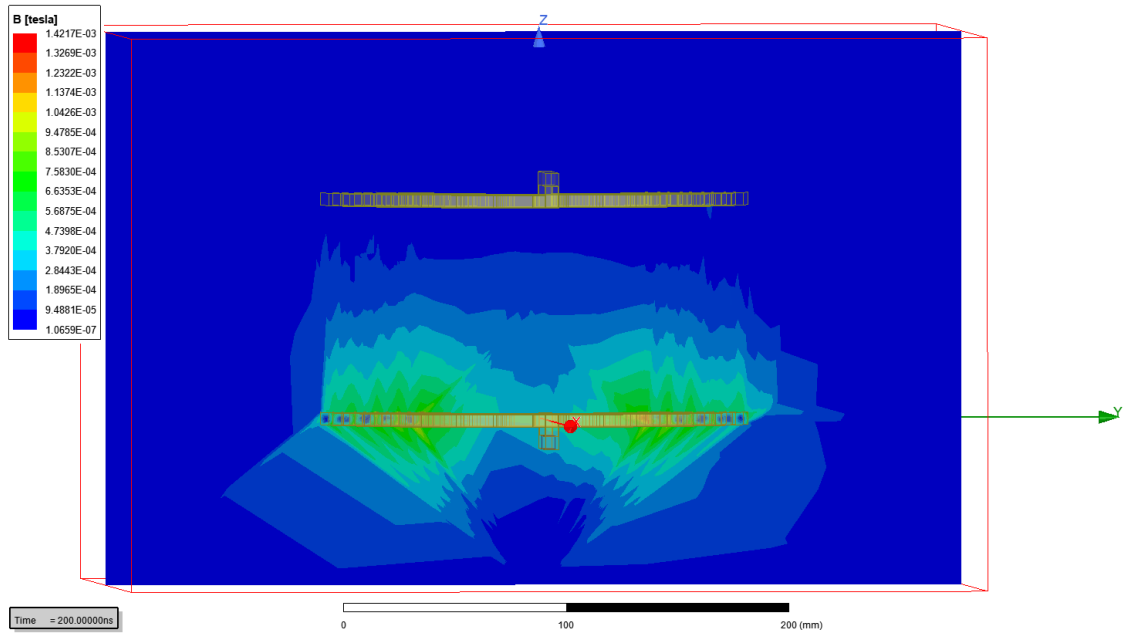
(a)
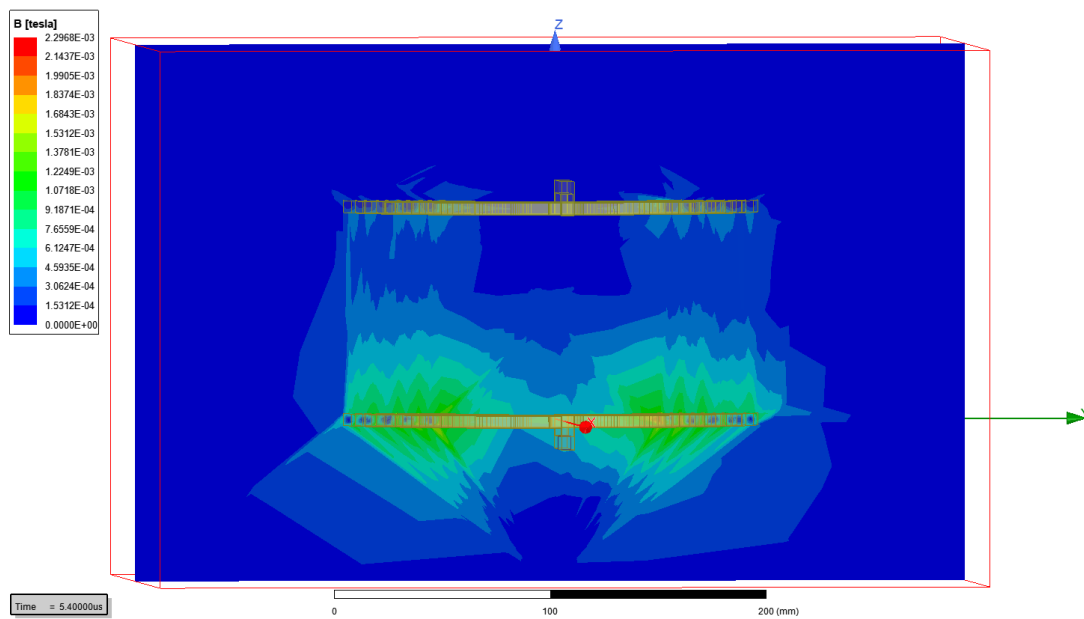
(b)

Figure 30 - the animation magnetic field in one period of Maxwell-Simplorer cosimualtion. (a) lowest value; (b) highest value
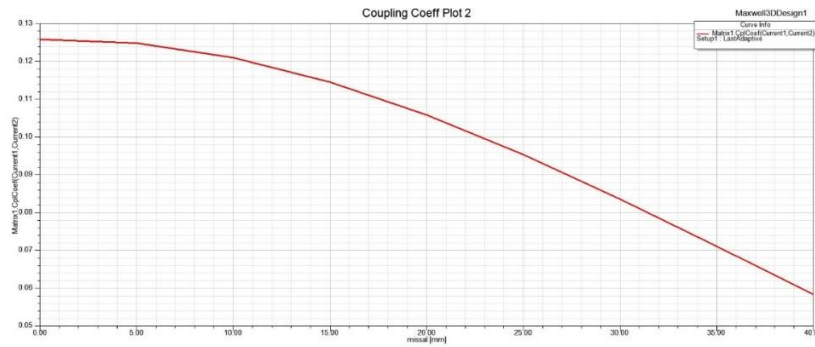
(a)
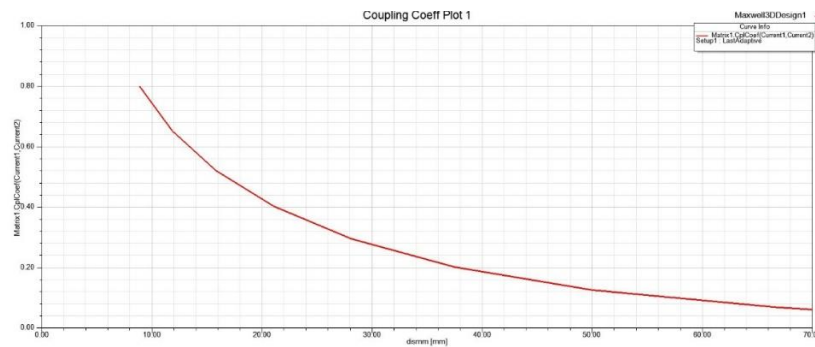
(b)

Figure 31 - Coupling coefficient versus: (a) coil distance; (b) misalignment

On the other hand, in order to optimize the parameters of whole circuit shown as Figure 32 where XFG1 signal generator is used to emulate the integrated circuit (IC) to control the switch of the buck DC-DC converter, both sides of WPT system are simulated by NI Multisim. The output voltage with different coupling coefficients which are 0.4, 0.6 and 0.8 is presented in Figure 33 whcih indicates that the output voltage is stablized at about 12 V with various coupling coefficient.
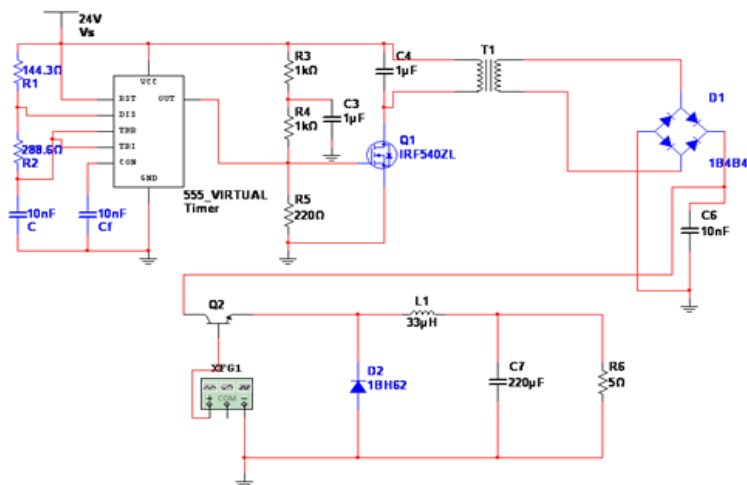
Figure 32- Circuit diagram of both sides.
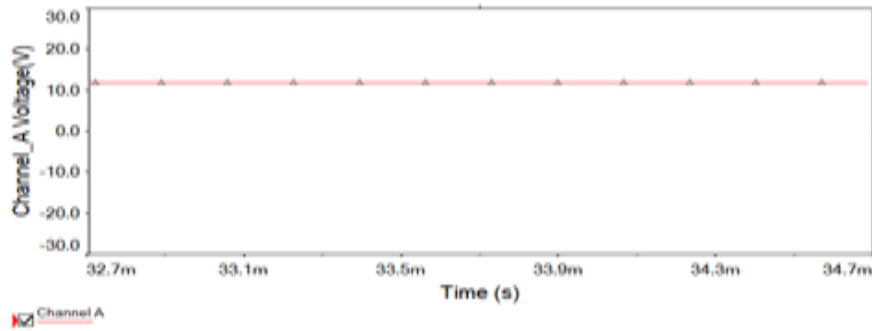
(a)
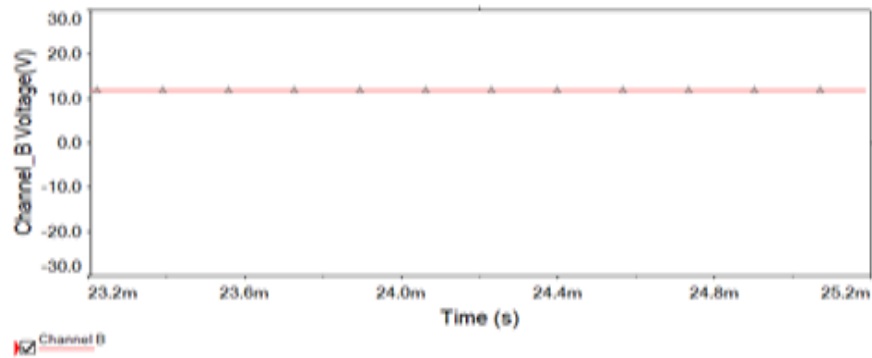
(b)
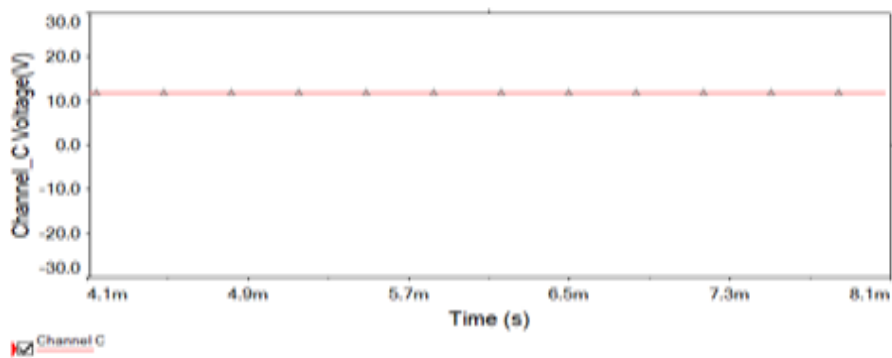
(c)

Figure 33- Steady state output voltage with different coupling coefficient; (a), (b) and (c) show output voltages under coefficients which are 0.4, 0.6 and 0.8 respectively

4.1.3. Improvement of Coil Structure Design

In oder to overcome the problem that coil coupling performance decrease under misalignment, two small Nd–Fe–B magnets are set on the center of two coils separately. When the hull flows through the arm of the power station, it will be caught by the

45

magnetic field and hold the charging position unless the propellers rotate with full speed again. According to [12], the magnets in such small size will not have significant influence on the electromagnetic field produced by Tx coli and the experiment results will be demonstrated to verify the point.

In some cases, human exposure issues have to be taken into accout since strong electromagnetic field (EMF) may cause damage to human health. Generally, the electromagnetic field is confirmed by power level and distance between human body and Tx coil. In this case, the out put power is only 36 W and the distance between charging station and human body is more than 2 m. Since the limits of human EMF exposure power indensity under 0.1 to 1 MHz is 9000 W/m^2 according to IEEE standard, obviously the human exposure in EMF in this case is small enough to be ignored.

4.1.4. Comparison Between Two Wireless Charging Platforms

In Figure 34, it presented the STEVAL-ISB047V1 wireless charger Tx evaluation kit which is based on STWBC-MC digital controller and MP-A15 3-coil array which can improve the performance under lateral misalignments. The output power is 15 W with extended input voltage in 5 to 20 V interval from USB-C or DC jack. The charger is certified by WPC Qi1.2.4 standard. Furthermore, it can realize foreign objective detection (FOD), active presence detection and robust demodulation algorithm [64].

Comparing the board with the WPT system proposed in this paper, the advantage of proposed system is that the output power in this case is 36 W which is much higher than that of WE board with a more compact dimension and simpler circuit structure. However, the performance against misalignment is not as good as triple-coil structure. Figure 35 and 36 show the block diagram and inductance curve versus frequency. In Figure 36, it can be seen that the inductance of the bottom coils and top coil are different because they partially overlap and induce mutual inductance, while the bottom inductance is a little higher the top. Furthermore, as the operation frequency increasing to more than 1000 kHz, the inductance of all three coils increases gradually while it keeps steady when the frequency is lower than 1000 kHz.
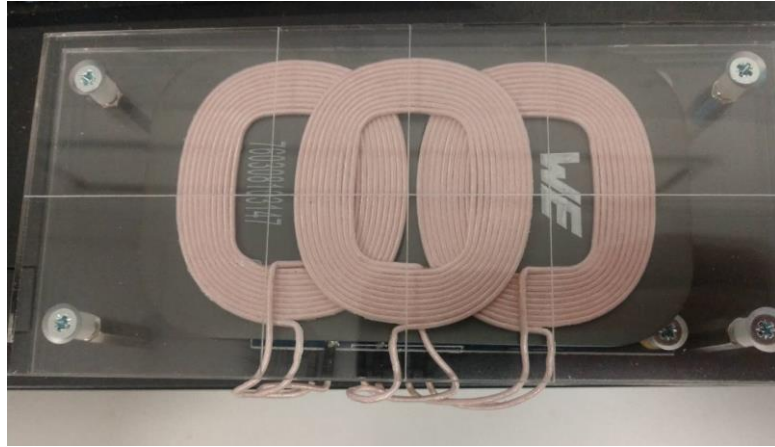
(a)
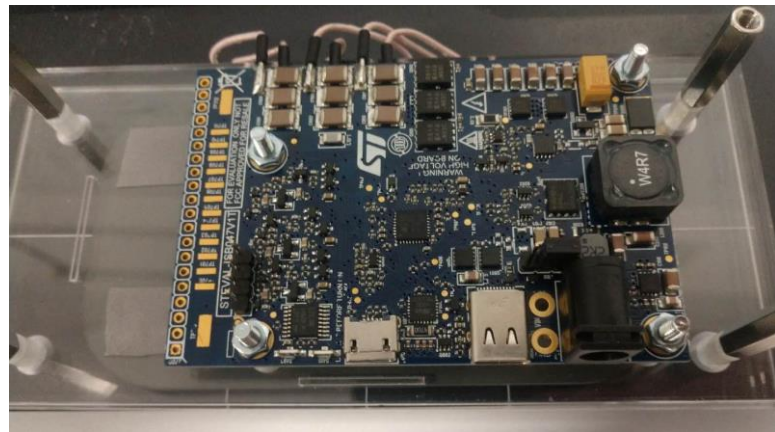
(b)

Figure 34－Coils and circuit of STEVAL-ISB047V1 wireless charger Tx
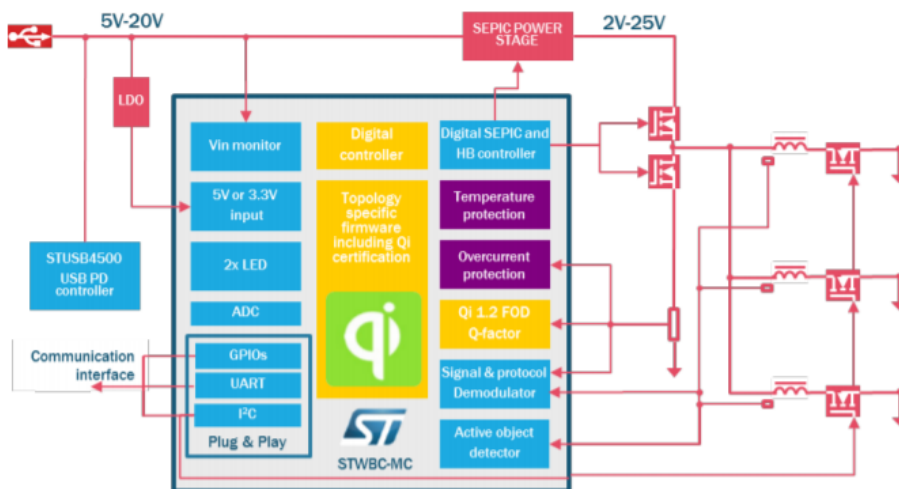
Figure 35 －Block diagrams of STEVAL-ISB047V1 wireless charger Tx
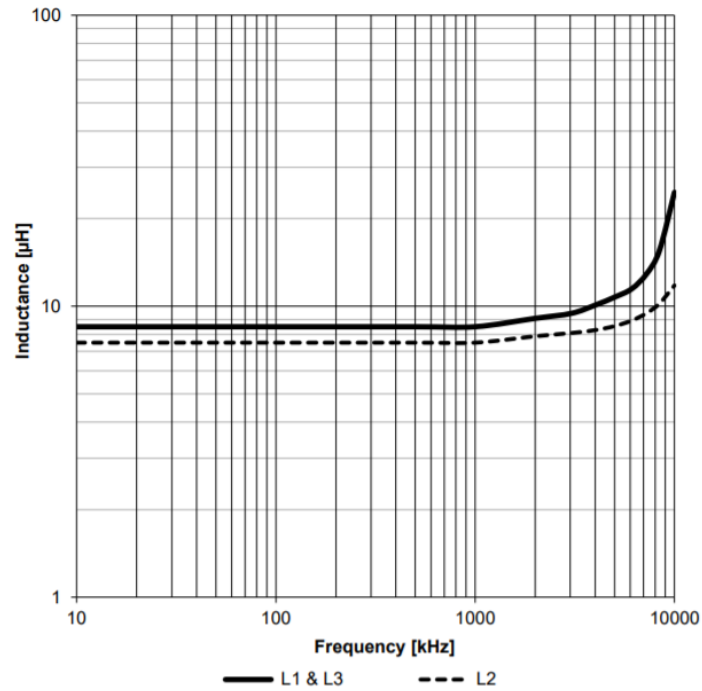
Figure 36 —Inductance curve versus frequency

4.1.5. Design of WPT Cahrging Station Mechanic Structure

In this section, it is concentrated on the mechanic structure design of the wireless charging station in which coils distance and misaliagnment is taken into account. At first, there was two proposals that one is to set the Rx coil at the bottom of the hull which means the Tx coil has to be immersed in the water and the other one is to set the Rx coil at the top of the hull while the Tx coil is fixed on the arm extending from the shore. Finally, the second proposal is taken in order to avoid under WPT which will cause eddy current loss and transmission efficiency decrease.

On the other hand, because the USV is underactuated, which is defined as a technical term used in robotics and control theory to describe mechanical systems that cannot be commanded to follow arbitrary trajectories in configuration space, propulsed by only two independent propellers, it is important to maintain the position of the hull to align the Rx and Tx coils so that the transmission efficiency can keep an ideal value. In this case, two magnets are set at the centre of two coils respectively to avoid misalignment. Such a solution has been recently utilized in Iphone 12, which is named Magsafe technology. In that case, it provides up to 15 W of power and is backwards-compactible with the open Qi standard for up to 7.5 W of power. Similar technology was firstly introduced in 2009 with PalmPre Touchstone system with a magnetically-attached wireless charger dock.

Figure 37 is the photo of Iphone 12 Magsafe disassembly. However, as a technology used in mobile communication devices, the biggest disadvantage of Magsafe is that it will demagnetize some magnetic cards when the device is close to the cards. Fortunately, in the case of USV wireless charging, it appearently does not need to be taken into consideration, so it is a simple, safe and highly efficient solution to use magnets to eliminate coil misalignment in USV wireless charging.

Figure 37 －Apple Magsafe disassembly

4.1.6. Wireless Charging Platform

In this case, the charging station is composed of an arm with Tx circuit and a bracket whose height can be adjusted via a stepper motor according to the coil distance measured by an ultrasonic sensor on the arm. In addition, the bracket on the shore is designed to be on the side of the hull since the DC brushless motors used in this case can only spin one-directional and the USV cannot go backwards. Figure 38 shows the relative position between the charging station and hull.
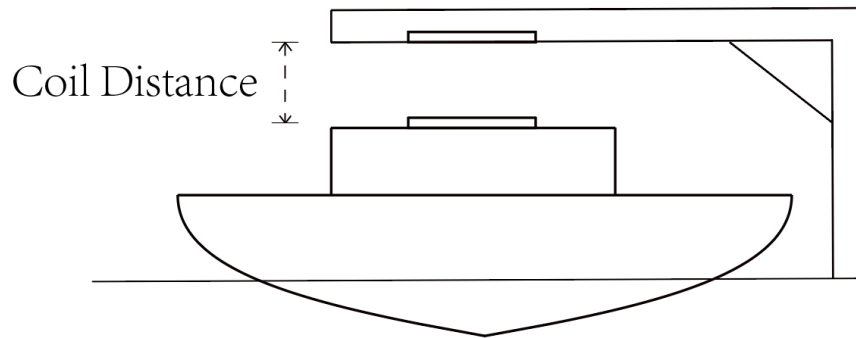
Figure 38- Coil distance and relative position relationship between charger and hull

Under actual circumstances, the water level changes with the tide which means that vertical position is not fixed. Thus, the platform with Tx coil should be designed to move with the hull vertically. A wooden experimental prototype of the WPT charging station was made in a studio and wood is chosen as the material because it has relatively low electrical conductivity and magnetic permeability that won't have effect on power transmission. Figure 39 and Figure 40 illustrate the process of bracket protocol and the protocol itself seperately.

Figure 39- Manufacture process
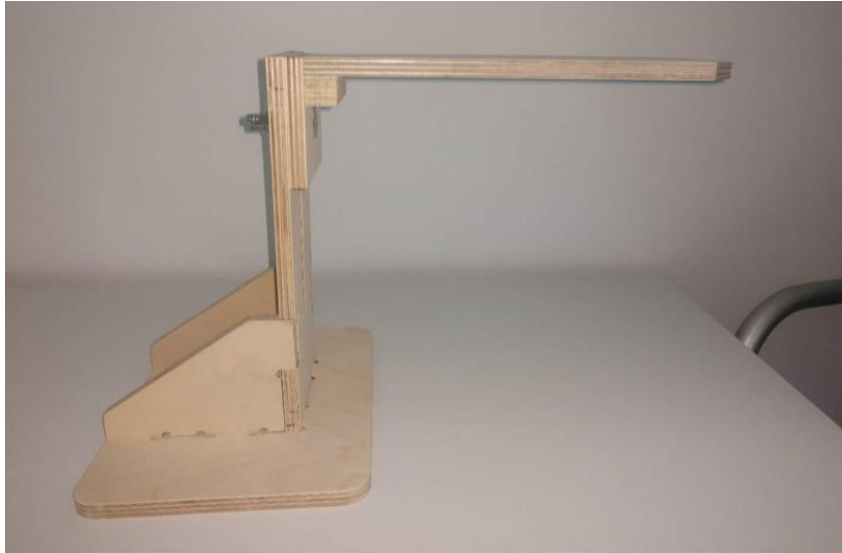
Figure 40- Bracket prototype

4.2. USV Moving Control

In this paper, the hull of the USV is cut out of a complete foam board and coated with black waterproof. The power source is a 3C, 2000 mAh LiPo battery. The USV is propulsed and headed by differencial thrust provided by two DC brushless motors. An Ultrasonic sensor working with a servo motor is utilized to realize obstacle avoidance. In addition, the whole motion control system is controlled by Arduino mega 2560 which can also receive instruction from host PC.

4.2.1. Moving Control method

There are two modes for the USV moving control which are automatic mode and remote controlling mode. In automatic mode, the USV will keep moving forward until the obstacle appears at 1 m ahead and then both two motors will stop rotation while the ultrasonic sensor spinning around with the servomotor to decide to turn left or right. The entired process will be cycled unless the mode is switched to remote control. Figure 41 is the flow chart of the motion system and Figure 42 shows the diagram of the automatic mode. The rotation speed of the motor is set to be as low as possible to save energy.
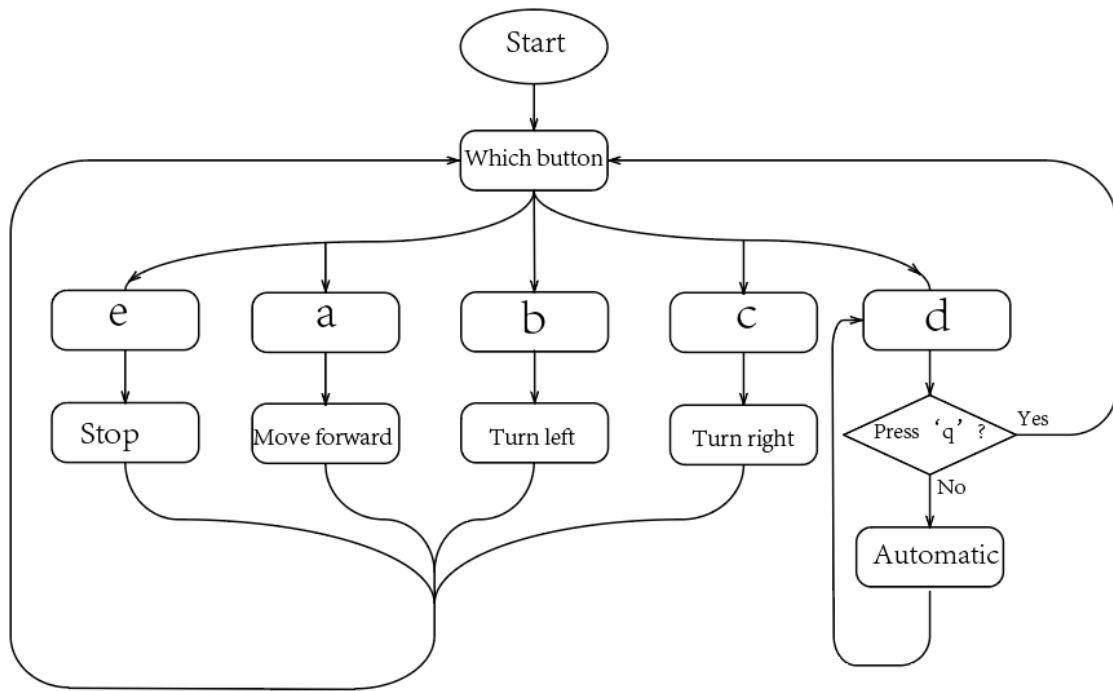
Figure 41- Diagram of motion system
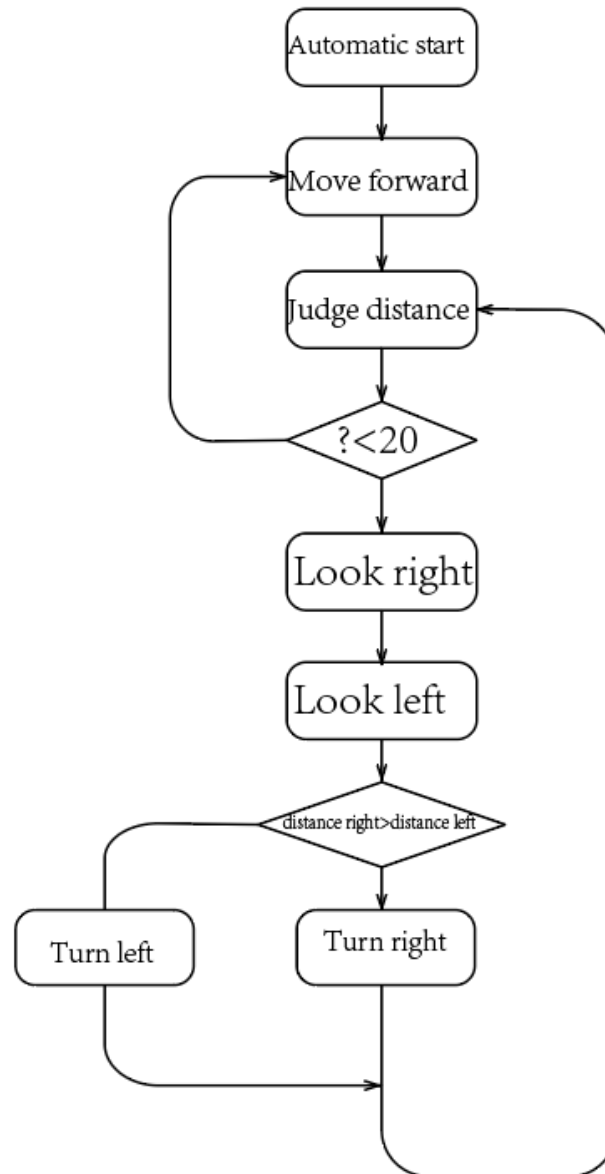
Figure 42- Diagram of automatic mode of USV moving

4.2.2. Battery Charge Management

It is known that it will reduce service life of LiPoly battery even raise safety issue if the battery is overcharged or overdischarged. As a result, it is quite essential to manage and monitor battery state in real time. To manage the battery energy, a simple battery manage system is developed. The voltage data detected by sensor are transferred to host PC through wireless data transmission module APC 220. Once the voltage is lower than 9 V, the alarm light in LabVIEW interface will be on to remind user to charge and it will not be off until the voltage is higher than 12.1 V. The process of battery management is illustrated in Figure 43.
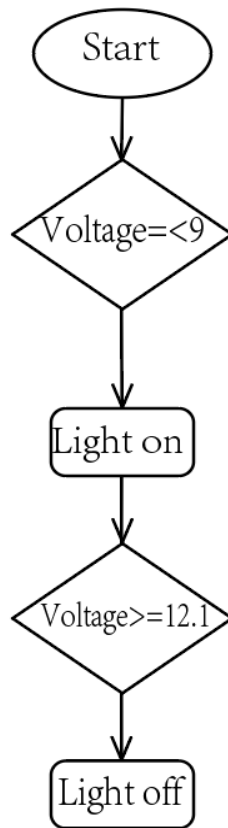
Figure 43- Diagram of battery management

4.2.3. Software

The complete process is programmed using IDE for Arduino and LabVIEW. In LabVIEW, a man-machine interface which is able to display data from the USV and control buttons were implemented. The programming diagrams of the program and the front panel are shown in Figure 44 and Figure 45 respectively. Figure 46 shows a part of Arduino code which is the code developed for remote control. The entire code will be shown in the Annex A.
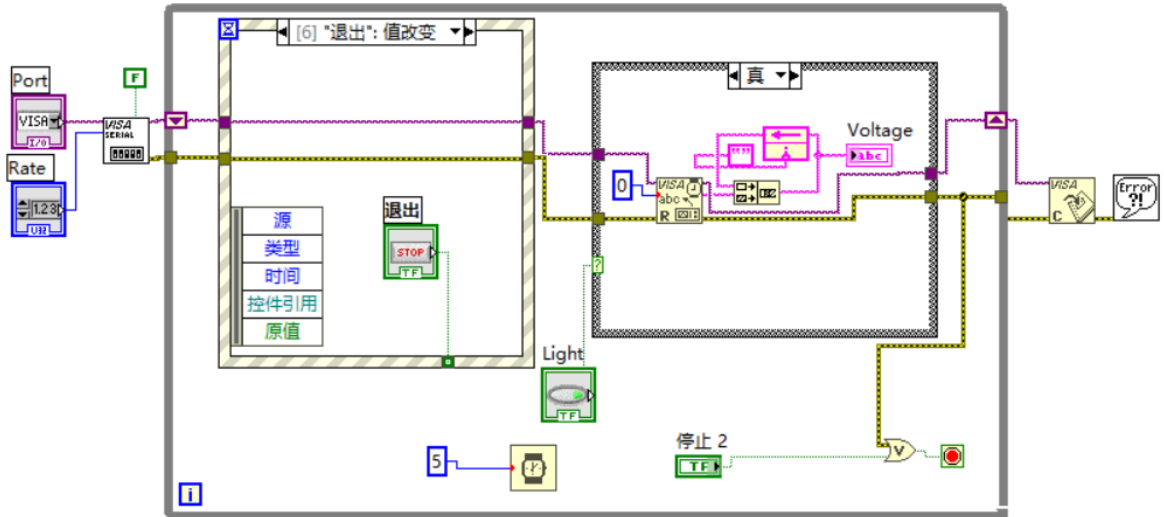
Figure 44- Diagram of program in LabView
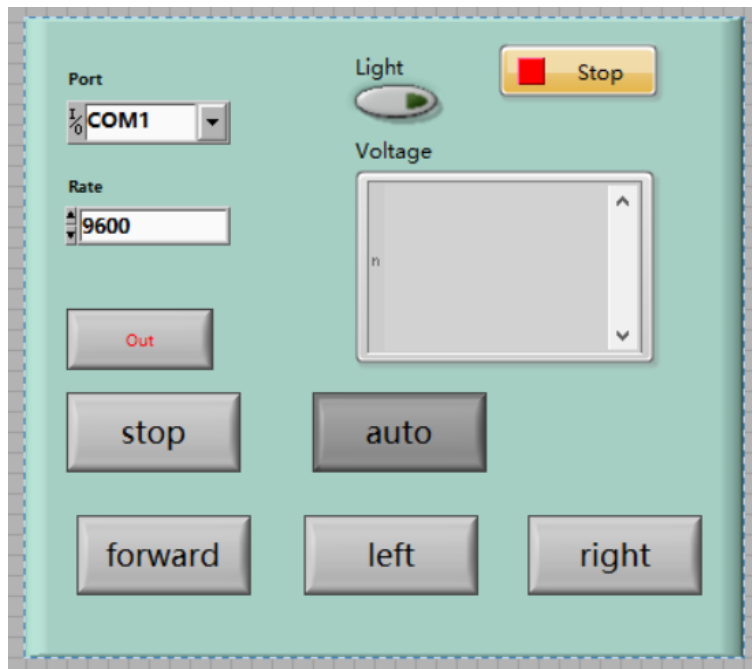
Figure 45- Diagram of front panel

```
if (distance<=20)
{
  esc_signal1.write(0);           //stop
  esc_signal.write(0);
  delay(300);
  distanceRight=LookRight();
  delay(300);
  distanceLeft=LookLeft();
  delay(300);

  if (distance>=distanceLeft)
  {
    esc_signal1.write(0);           //turn right
  esc_signal.write(63);
  esc_signal1.write(0);           //stop
  esc_signal.write(0);
  }
  else
  {
    esc_signal1.write(62);          //turn left
  esc_signal.write(0);
  esc_signal1.write(0);           //stop
  esc_signal.write(0);
  }
}
else{
  esc_signal1.write(62);  //forward
  esc_signal.write(63);
}
distance=readPing();
```

Figure 46- Part of Arduino code for USV remote control

Chapter 5 – Experimental Results and Discussion

In previous section, both coil coupling and circuit simulation are given to indicate the relationship between relative coils position and coupling coefficient as well as the result of circuit design. In this section, it is focused on experiment description mainly composed of experiment devices, method and experiment results comparison analysis in different conditions.

5.1. Experiment for WPT circuits

5.1.1. Experimental Setup

In this case, an experiment is set up to verify the validation of the WPT system. The complete experiment devices are constituted by a DC voltage source (BK PRECISION 912B), a wireless charging module whose circuit design diagram is shown in Figure 31 including transmitting and receiving sides, a KEITHLEY 2000 multimeter, a KEYSIDHT DSOX1102A digital storage oscillope and an 11.1 V 2200 mAh Li-PO battery as the load. Figure 47 is a photo of the whole experiment system. Table 12 shows the parameters of the proposed WPT circuit.

Table 12 – Parameters of the WPT system

Components	Parameters	Values
Tx coil	L_p	14 μH
	C_p	70 μF
	ω_0	200 kHz
Rx coil	L_s	14 μH
	C_s	70 μF
	ω_0	200 kHz

During the experiment, the DC voltage source feeds 24 V voltage and 1.5 A current to the Tx of the WPT system. The experiment is processed in open circuit at first and then with load to gain voltage and current data in two different situations by multimeter and oscilloscope.
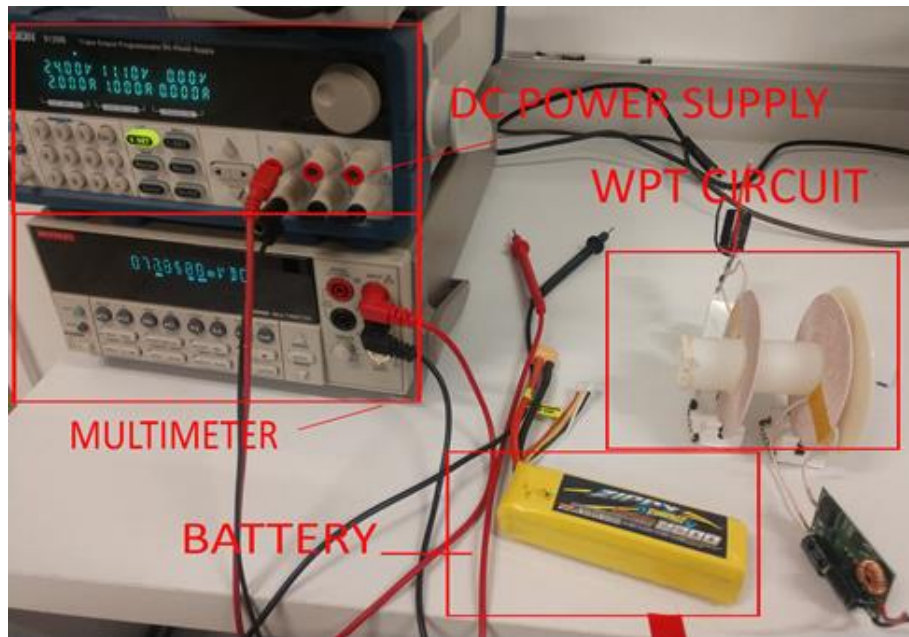
Figure 47- The experiment devices.

5.1.2. Experiment Results Analysis

First, the voltage on the Tx coil without transferring power to the Rx coil is measured by the oscillope. The voltage waveform is demonstrated in Figure 48 and 49. It can be seen that the operation frequency gets to 141.64kHz and Pk-Pk value gets to 892V which indicates that the inverter circuit has a good performance on power inverting and amplifying. Second, the Rx coil is set 1cm away from the Tx coil axially and the voltage waveform on the Tx and Rx coils are illustrated in Figure 48 which can be seen that as the power transferred to the Rx circuit, the Pk-Pk voltage on the Tx coil decreases to 788V. The sinwaveform of the Rx coil voltage differs from that of the Tx coil by a half cycle, which indicates that the rectifier and buck converter achieve performance indicators.
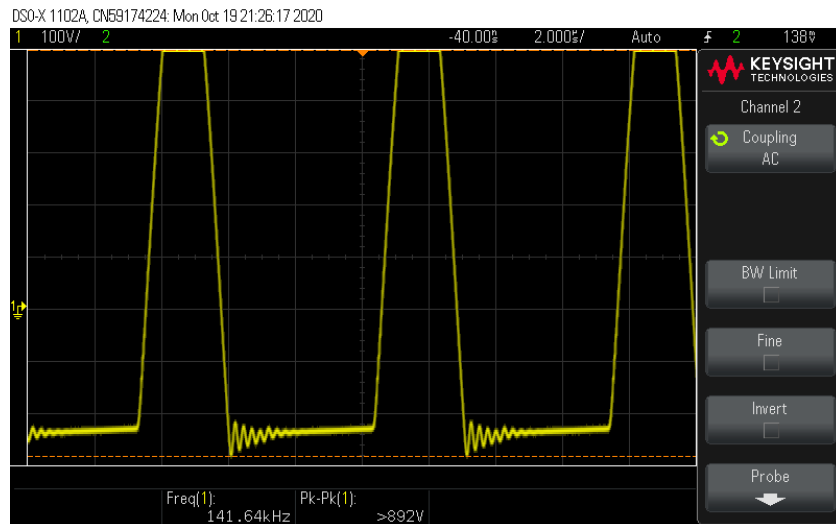
Figure 48- Tx coil voltage without Rx circuit
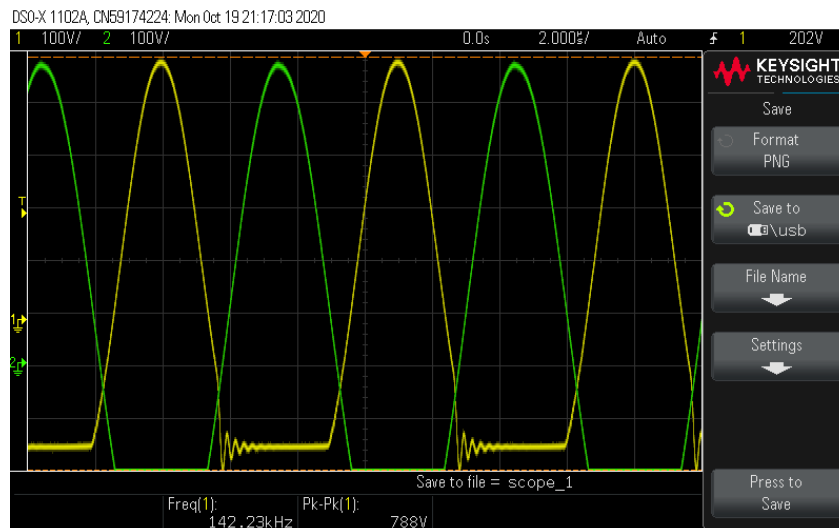
Figure 49- Voltage on Tx and Rx coil when well coupled

1) Open Circuit Situation: First, the voltage variations versus different colis distance and misaliagnment are researched. In this experiment, two coils are moved coaxially to change the distance between. Then, the coils are set to be 3 cm far and moved parallel to change the misalignment. The results are shown in Figure 50. It can be seen that the voltage when coaxial stabilizes at about 12 V between 2.5-6.5 cm and decreases gradually while the distance is longer than 6.5 cm. However, the voltage with misalignment is stable when the misalignment is smaller than 5 cm and then attenuates severely. Considering the diameter of the coils is only 8.2 cm, not so large compared to the distance in the experiment, the voltage stabilization of the proposed WPT system is basically satisfied.
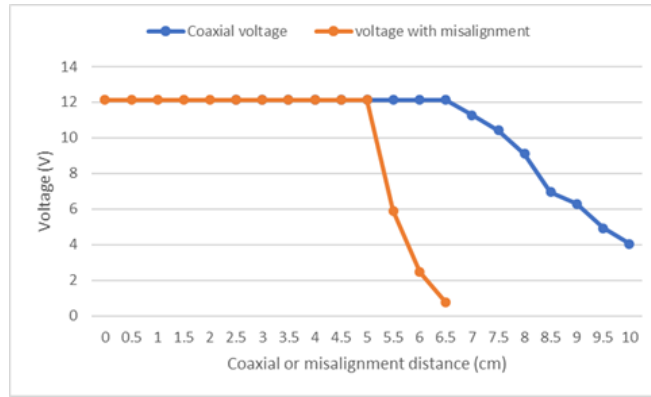
Figure 50- Open circuit voltage versus coils distance.

2) Experiment with Load: When a 3C, 11.1V, 2200mAh LiPo battery is connected to the second side as the load, the current under different coupled index can be got. Thus, the power transmission efficiency can be derived by as follows:

$$\eta = \frac{P_{out}}{P_{in}} = \frac{U_{out}I_{out}}{U_{in}I_{in}} \tag{13}$$

Where P_{in} and P_{out} are input and output power, I_{in} and I_{out} are input and output current, U_{in} and U_{out} are input and output voltage, respectively. The results of the current and power efficiency are shown in Figure 51 and Figure 52, separately.
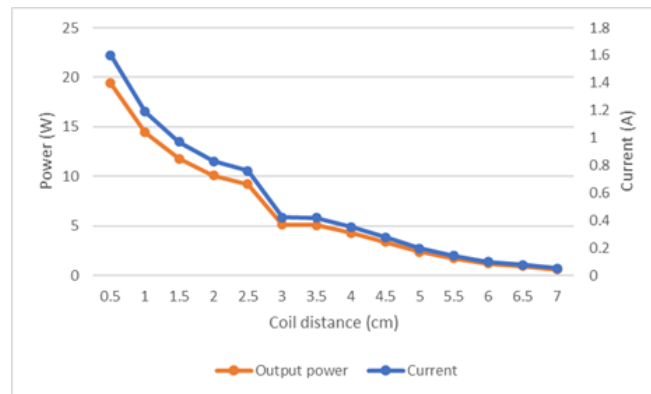
Figure 51- Current and output power value with battery load versus Rx-Tx coil distance
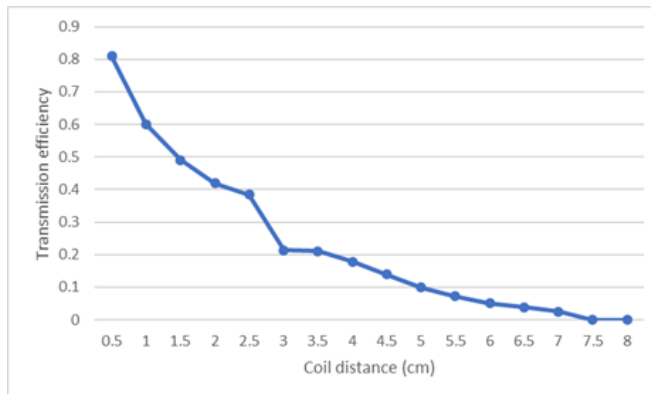
Figure 52- Power transmission efficiency versus Rx-Tx coil distance

In Figure 50, it presents that the highest current 1.6 A and output power 19.4 W can be got when the distance is 0.5 cm and then it reduces as the distance keeps increasing. Meanwhile, the peak of power transmission efficiency reaches 80.6% at 0.5 cm as shown in Figure 51 and the trends of current, output power and power transmission curves going down with Tx-Rx distance increasing are basically the same, which corresponds to (13). Just in case the circuit of receiver is overloaded, the distance between coils can't be smaller than 0.5 cm. Since the voltage is stable at 12 V in the range of 0.5 to 7 cm, it means the output power and efficiency will decrease with the current. The errors in the experiment mainly are caused by measuring operation.

5.2. Experiment for Charging USV on Water

5.2.1. Experimental Setup

The final experiment was carried out in a plastic water tank whose dimensions are 94 X 55 X 53 [cm] to verify the availability of the WPT charging station and the water inside is 6 cm deep. During the experiment, the charging bracket is hung on the rampart of the tank by a rope. All the hardware on the USV is packed in a plastic box to keep waterproof. Then height of the charging arm can be changed to get the best charging efficiency. The photo of water experimental setup is shown in Figure 53.
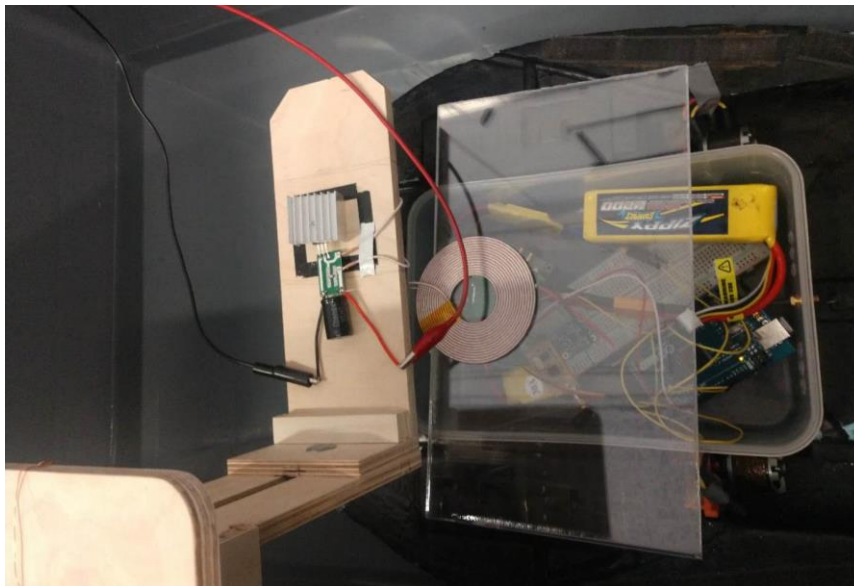
Figure 63- Wireless power station demonstration

Due to fluid properties of water, it is hard to fix the position of the USV. Thus, two magnets are set on the center of the coils to catch and hold the Rx coil. The experiment

shows that the Rx coil can be caught when the Rx coil is 2 cm at most misaligned from the charging center and can keep steady in flowing water. In addition, an HC-RS is sticked on the charging arm in order to measure the distance between two coils.

5.2.2. Experimental Result Analysis

First, the power of the battery was cosumed to 8.1 V which is set to be the lowest safety voltage. Then, it started to charge while the voltage and corresponding time was recorded until the voltage got to 12.1 V. The experiment was carried out when coil distances are 0.5, 1 and 1.5 cm respectively. The results are shown in Figure 54 which indicates that the battery is fully charged in 2 hours when the axcial coil distance is 1cm and the charging rate from 8.1 to 10 V is higher than that from 10 to 12.1 V due to the battery charging property. The experiment proves the validation of the WPT charging system for the battery which is the USV power supply. However, if the distance between Tx and Rx coils, the output voltage will be too low to charge the battery.
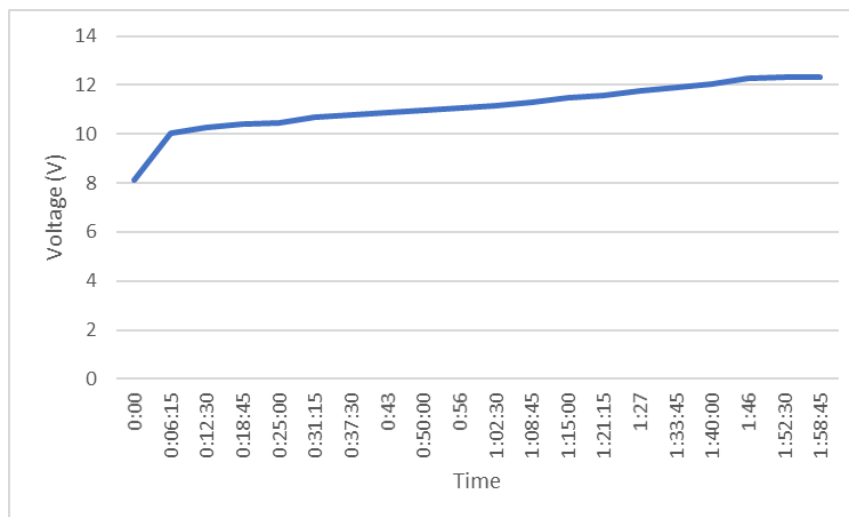
Figure 74- Battery voltage vs time in 2 h

Chapter 6 – Conclusions and Future Work

6.1. Conclusions

A WPT charging system for USV including the performance evaluation was designed and implemented, which is the main goal of the dissertation. The main work focuses wireless charging design, while remote control and obstacle ovoidance are minor.

The system capabilities were tested and the obtained data allows to compared the results coming from different charging distance and coils misalignments. With the analysis of tha data, the validation of the proposed WPT circuit is certificated. The dissertation also provides a mechanical protocol design which is made wood considering the feature of USV motion. To combat lateral misalignment, coils with Nd–Fe–B magnets are designed and the its influence on Tx coil electromagnetic field is analysed through experiment. Finally, the charging time for LiPoly battery from 9.0 to 12.1 V is recorded, which indicates the validation of the proposed charging circuit. In addition, other basic functions of the USV are well integrated such as obstacle ovoidance, remote control and data upload, which is tested through the experiment.

At the technological level, the WPT circuit is designed into a very small size, which make it easy to be used into most kinds of applications, especially those which have small inner space. Meanwhile, the voltage stabilization of the circuit gets an ideal result which can be stable at a certain value in a range of misalignment.

In this work, the validation of WPT system for USVs is verified which indicates that WPT can be a promising technology not only to those applications on land such as EV (electric vehicle) and mobile communication devices but also to those water equipments like USVs.

6.2. Contributions

This implemented MSc work presents a WPT system which can supply a stable 12 V voltage and achieve around 80.6% highest power transmission efficiency with micro frequency control chips, XKT-801 and XKT-3170, which reduces the circuit size obviously and makes it easier to be applied in small space. The module of circuit is adapted to analyze the system. The experiment is brought out to prove the validation of the system. The results show that the proposed system has a good performance in terms of output voltage sensitivity reduction.

6.3. Future Work

Despite being a fairly comprehensive system, improvements can still be made, both software and hardware.

To software, the interface made by LabVIEW is easy to operate, however it lacks aesthetics and can be improved.

To hardware, the WPT charging circuit proposed can only realize constant voltage charging, but no constant current charging which can be achieved by switching circuit.

As even further work, the characteristics of WPT system for underwater applications will considering the underwater automatic vehicle development since the previous work is still on WPT in the air which has been studied a lot. For example, there are different characteristics in different kinds of natural water. It is known that the conductivity, permeability and permittivity of lake and oceans of various areas has enough differences to influence eddy current loss because of ion concentration. Usually, sea water of which conductivity is 50 mS/cm causes higher eddy current loss than other water or air due to its salt content. Additional experiments can be done to test the transmission effect of different media such as air, plastic, medal, water with different salinity, etc.

There is still much space for development on underwater wireless power transfer (UWPT) such as the calculation of eddy current loss in sea water as well as design of UWPT station.

Reference

1- S. Shin et al., "Wireless power transfer system for high power application and a method of segmentation," 2013 IEEE Wireless Power Transfer (WPT), Perugia, 2013, pp. 76-78, doi: 10.1109/WPT.2013.6556886.

2- Seokhwan Lee et al., "The optimal design of high-powered power supply modules for wireless power transferred train," 2012 Electrical Systems for Aircraft, Railway and Ship Propulsion, Bologna, 2012, pp. 1-4, doi: 10.1109/ESARS.2012.6387396.

3- J. H. Kim et al., "Development of 1-MW Inductive Power Transfer System for a High-Speed Train," in IEEE Transactions on Industrial Electronics, vol. 62, no. 10, pp. 6242-6250, Oct. 2015, doi: 10.1109/TIE.2015.2417122.

4- Y. Zhang, T. Lu, Z. Zhao, F. He, K. Chen and L. Yuan, "Selective Wireless Power Transfer to Multiple Loads Using Receivers of Different Resonant Frequencies," in IEEE Transactions on Power Electronics, vol. 30, no. 11, pp. 6001-6005, Nov. 2015, doi: 10.1109/TPEL.2014.2347966.

5- C. Cheng, Z. Zhou, W. Li, C. Zhu, Z. Deng and C. C. Mi, "A Multi-Load Wireless Power Transfer System With Series-Parallel-Series Compensation," in IEEE Transactions on Power Electronics, vol. 34, no. 8, pp. 7126-7130, Aug. 2019, doi: 10.1109/TPEL.2019.2895598.

6- C. Cheng et al., "Load-Independent Wireless Power Transfer System for Multiple Loads Over a Long Distance," in IEEE Transactions on Power Electronics, vol. 34, no. 9, pp. 9279-9288, Sept. 2019, doi: 10.1109/TPEL.2018.2886329.

7- X. Zhang, X. Zhang and L. Han, "An Energy Efficient Internet of Things Network Using Restart Artificial Bee Colony and Wireless Power Transfer," in IEEE Access, vol. 7, pp. 12686-12695, 2019, doi: 10.1109/ACCESS.2019.2892798.

8- J. Guo, L. Tan, H. Liu, W. Wang and X. Huang, "Stabilization Control of Output Power in Double-Source Wireless Power Transfer Systems Without Direct Output Feedback," in IEEE Microwave and Wireless Components Letters, vol. 26, no. 11, pp. 960-962, Nov. 2016, doi: 10.1109/LMWC.2016.2615026.

9- Y. Zhang, T. Lu, Z. Zhao, K. Chen, F. He and L. Yuan, "Wireless Power Transfer to Multiple Loads Over Various Distances Using Relay Resonators," in IEEE

Microwave and Wireless Components Letters, vol. 25, no. 5, pp. 337-339, May 2015, doi: 10.1109/LMWC.2015.2409776.

10- A. Rajvanshi," Nikola Tesla- The Creator of Electric Age," Resonance, March 2007.

11- S. Lukic, Z. Pantic," Cutting the Cord: Static and Dynamic Inductive Wireless Charging of Electric Vehicles," IEEE Electrification Magazine, pp. 57-64, 2013.

12- S. Hui, W. Ho,"A New Generation of Universal Contactless Battery Charging Platform for Portable Consumer Electronic Equipment," IEEE Trans. on Power Electron., vol. 20, no. 3, pp: 620-627, 2005.

13- B. Choi, J. Nho, H. Cha, et al.,"Design and Implementation of Low-profile Contactless Battery Charger Using Planar Printed Circuit Board Wingdings as Energy Transfer Device," IEEE Trans. on Industrial Electron., vol. 51, no. 1, pp. 140-147, 2004.

14- S. Lee, G. Choi, S. Choi, T. Nguyen, and T. Rim," Wide-Range Adaptive IPT Using Dipole-Coils with a Reflector by Variable Switched Capacitance," IEEE Trans. on Power Electron., vol. 32, no. 10, pp. 8054-8070, Oct. 2017.

15- S. Ding, W. Niu, and W. Gu," Lateral Misalignment Tolerant Wireless Power Transfer with a Tumbler Mechanism," IEEE Access, vol. 7, pp. 125091-125100, August 2019.

16- Z. He, Y. Wang, L. Ding, and X. Nie," Research on Three-Dimensional Omnidirectional Wireless Power Transfer System for Subsea Operation," OCEANS 2017-Aberdeen, UK, June 1017.

17- O. Abdelatty, X. Wang, and A. Mortazawi," Position-Insensitive Wireless Power Transfer Based on Nonlinear Resonant Circuits," IEEE Trans. on Microwave Theory and Techniques., vol. 67, no. 9, pp. 3844-3855, March 2019.

18- W. Zhang, and C. Mi," Compensation Topologies of High-Power Wireless Power Transfer Systems," IEEE Trans. on Vehicular Technology., vol. 65, no. 6, pp. 4768-4778, June 2016.

19- J. Lee, K. Lee, and D. Cho," Stability Improvement of Transmission Efficiency based on Relay Resonator in Wireless Power Transfer System," IEEE Trans. on Power Electron., vol.32, no. 5, pp. 3297-3300, May 2017.

20- W. Niu, J. Wang, J. Chu, W. Gu," Optimal single relay position of a 3-coil wireless power transfer system," The Journal of Engineering, vol. 2016, no. 7, pp. 249-252, July 2016.

21- J. Agbinya, and H. Nguyen," Principles and Applications of Frequency Splitting in Inductive Communications and Wireless Power Transfer Systems," Wireless Personal Communications, vol. 107, pp. 987-1017, April 2019.

22- Y. Zhang, T. Kan, Z. Yan, Y. Mao, Z. Wu, and C. Mi," Modeling and Analysis of Series-None Compensation for Wireless Power Transfer Systems with a Strong Coupling," IEEE Trans. on Power Electron., vol. 34, no. 2, pp.1209-1215, Feb. 2019.

23- A. Ramezani, S. Farhangi, H. Eini, B. Farhangi, R. Rahimi, and G. Moradi," Optimized LCC-Series Compensated Resonant Network for Stationary Wireless EV Charger," IEEE Trans. on Industrial Electron., vol. 66, no. 4, pp. 2756-2765, June 2018.

24- B. J. Varghese, T. Smith, A. Azad and Z. Pantic, "Design and optimization of decoupled concentric and coplanar coils for WPT systems," 2017 IEEE Wireless Power Transfer Conference (WPTC), Taipei, 2017, pp. 1-4, doi: 10.1109/WPT.2017.7953838.

25- "Underwater observatory (OBSEA)", [Online]. Available: https://www.upc.edu/sct/en/equip/73/underwater-observatory-obsea.html [Accesses: 17-Nov- 2020]

26- W. Niu, W. Gu and J. Chu, "Experimental investigation of frequency characteristics of underwater wireless power transfer," 2018 IEEE MTT-S International Wireless Symposium (IWS), Chengdu, 2018, pp. 1-3, doi: 10.1109/IEEE-IWS.2018.8400876.

27- Song Xianjin, Liu Guoqiang, Li Yanhong, Zhang Chao and Xu Xiaoyu, "Analyses and experiments of field-circuit coupling equations for wireless power transfer using solenoidal coils," 2015 IEEE International Wireless Symposium (IWS 2015), Shenzhen, 2015, pp. 1-4, doi: 10.1109/IEEE-IWS.2015.7164593.

28- Z. Yan, B. Song, Y. Zhang, K. Zhang, Z. Mao and Y. Hu, "A Rotation-Free Wireless Power Transfer System With Stable Output Power and Efficiency for Autonomous Underwater Vehicles," in IEEE Transactions on Power Electronics, vol. 34, no. 5, pp. 4005-4008, May 2019, doi: 10.1109/TPEL.2018.2871316.

29- I. F. Lopes, R. Lacerda Valle, G. Azevedo Fogli, A. A. Ferreira and P. Gomes Barbosa, "Low-Frequency Underwater Wireless Power Transfer: Maximum Efficiency Tracking Strategy," in IEEE Latin America Transactions, vol. 18, no. 07, pp. 1200-1208, July 2020, doi: 10.1109/TLA.2020.9099760.

30- J. E. Manley," Unmanned maritime vehicles, 20 years of commercial and technical evolution", In OCEANS 2016 MTS/IEEE Monterey, pages 1–6, 201.

31- H. Ashrafiuon, K. R. Muske, and L. C. McNinch. Review of nonlinear tracking and setpoint control approaches for autonomous underactuated marine vehicles. In Proceedings of the 2010 American Control Conference, pages 5203–5211, 20

32- Y. Wang, J. Shen, and X. Liu. Dynamic obstacles trajectory prediction and collision avoidance ofusv. In2017 36th Chinese Control Conference (CCC), pages 2910–2914, 20.

33- "A* search algorithm", [Online]. Available: https://en.wikipedia.org/wiki/A*_search_algorithm#:~:text=A*%20is%20an%20informed%20search,shortest%20time%2C%20etc.). [Accesses: 17-Nov-2020].

34- M. Liu, S. Yang, H. Si, and Z. Zou. The preliminary optimization analysis of a high-speed monohullusv's propulsion system. In 2016 Asia-Pacific Conference on Intelligent Robot Systems (ACIRS), pages 149–157, 201.

35- "Connectivity of the Internet of Things", [Online]. Available: http://blog.gridconnect.com/blog/general/connectivity-of-the-internet-of-things. [Accessed: 26-Oct-2020].

36- J. Lee, Y. Su, and C. Shen," A Comparative Study of Wireless Protocols: Bluetooth, UWB, ZigBee, and Wi-Fi", IECON Proc. Industrial Electron. Conf., vol. 4, no. 6,pp.46-51,2014.

37- M. Liu, S. Yang, H. Si, and Z. Zou. The preliminary optimization analysis of a high-speed monohullusv's propulsion system. In2016 Asia-Pacific Conference on Intelligent Robot Systems (ACIRS), pages 149–157, 201

38- C. Gezer, M. Niccolini, and C. Buratti. An ieee 802.15.4/zigbee based wireless sensor network forenergy efficient buildings. In 2"010 IEEE 6th International Conference on Wireless and Mobile Com-puting, Networking and Communications, pages 486–491, 20.

39- "APC Series Transparent Transceiver Module APC220-43", Data sheet.

40- "What is Arduino?" [Online]. Available: https://www.arduino.cc/en/guide/introduction. [Access: 26-Oct-2020].

41- " Arduino Compare board specs". [Online]. Available: https://www.arduino.cc/en/products/compare. [Access: 26-Oct-2020].

42- A. Nayyar and V. Puri, "A review of Arduino board's, Lilypad's & Arduino shields," *2016 3rd International Conference on Computing for Sustainable Global Development (INDIACom)*, New Delhi, 2016, pp. 1485-1492.

43- N. Miyanaga, T. Inoue, H. Yoshida, K. Komada and M. Goto, "Large scale lithium-ion battery cells for space use," The 25th International Telecommunications Energy Conference, 2003. INTELEC '03., Yokohama, Japan, 2003, pp. 241-248.

44- G. Feng, L. Liu, W. Cui, R. Wang and T. Hu, "Transient Characteristics of Charging Effects due to E-Beam Irradiation: A Method of SEY-Based Charging Balance Mode," in IEEE Transactions on Plasma Science, vol. 47, no. 8, pp. 3783-3789, Aug. 2019, doi: 10.1109/TPS.2019.2919874.

45- H. A. Yiğit, H. Uluşan, S. Chamanian and H. Külah, "Charge Balance Circuit for Constant Current Neural Stimulation with Less than 8 nC Residual Charge," 2019 IEEE International Symposium on Circuits and Systems (ISCAS), Sapporo, Japan, 2019, pp. 1-5, doi: 10.1109/ISCAS.2019.8702790.

46- S. J. Thomson, P. Thomas, A. R. and E. Rajan, "Design and Prototype Modelling of a CC/CV Electric Vehicle Battery Charging Circuit," 2018 International Conference on Circuits and Systems in Digital Enterprise Technology (ICCSDET), Kottayam, India, 2018, pp. 1-5, doi: 10.1109/ICCSDET.2018.8821071.

47- S. Anbu Yazhini and D. S. Harish Ram, "High level synthesis of data flow graphs using integer linear programming for switching power reduction," 2011 International Conference on Signal Processing, Communication, Computing and Networking Technologies, Thuckafay, 2011, pp. 475-479, doi: 10.1109/ICSCCN.2011.6024597.

48- F. Li, A. Pop and A. Cohen, "Automatic Extraction of Coarse-Grained Data-Flow Threads from Imperative Programs," in IEEE Micro, vol. 32, no. 4, pp. 19-31, July-Aug. 2012, doi: 10.1109/MM.2012.49.

49- K. R. Asha, P. S. Tasleem, A. V. Ravi Kumar, S. M. Swamy and K. R. Rekha, "Real Time Speed Control of a DC Motor by Temperature Variation Using LabVIEW and Arduino," 2017 International Conference on Recent Advances in Electronics and Communication Technology (ICRAECT), Bangalore, 2017, pp. 72-75, doi: 10.1109/ICRAECT.2017.50.

50- R. M. Shrenika, S. S. Chikmath, A. V. R. Kumar, Y. V. Divyashree and R. K. Swamy, "Non-contact Water Level Monitoring System Implemented Using LabVIEW and Arduino," 2017 International Conference on Recent Advances in Electronics and Communication Technology (ICRAECT), Bangalore, 2017, pp. 306-309, doi: 10.1109/ICRAECT.2017.51.

51- Z. Adel, A. A. Hamou and S. Abdellatif, "Design of Real-time PID tracking controller using Arduino Mega 2560for a permanent magnet DC motor under real disturbances.," 2018 International Conference on Electrical Sciences and Technologies in Maghreb (CISTEM), Algiers, 2018, pp. 1-5, doi: 10.1109/CISTEM.2018.8613560.

52- S. B. Jarad, V. D. Lohar, S. P. Choukate and S. D. Mangate, "Automatic Optimization and Control of Power Factor, Reactive Power and Reduction of THD for Linear and Nonlinear Load by Using Arduino UNO," 2018 Second International Conference on Inventive Communication and Computational Technologies (ICICCT), Coimbatore, 2018, pp. 1128-1132, doi: 10.1109/ICICCT.2018.8473191.

53- "NTM Prop Drive Series 28-30A 750kv / 140w" [Online]. Available: https://hobbyking.com/en_us/ntm-prop-drive-series-28-30a-750kv-140w.html?___store=en_us. [Access: 31-Oct-2020]

54- "HW30A 30A Brushless Motor ESC" [Online]. https://www.amazon.com/QUAKOI-HW30A-Brushless-Airplane-Quadcopter/dp/B082M9HNV9. [Access: 31-Oct-2020]

55- "Ultrasonic Ranging Module HC - SR04" [Datasheet].

56- "SG90 Digital" [Datasheet online]. Available: http://www.towerpro.com.tw/product/sg90-7/. [Access:1-Nov-2020]

57- "ZIPPY Compact 2200mAh 3S 25C Lipo Pack" [Online]. Available: https://circuit.rocks/product:2536. [Access: 1-Nov-2020]

58- "Voltage Sensor Module" [Online] https://components101.com/sensors/voltage-sensor-module. [Access: 1-Nov-2020]

59- G. Qiu,"Circuit," China: Hingher Education Press, June 2006.

60- S. Fan, Y. Yu, Y. Zhang and H. Yang, "Multi-mode Synchronized PWM Schemes for three-level NPC Inverter," 2019 22nd International Conference on Electrical Machines and Systems (ICEMS), Harbin, China, 2019, pp. 1-5, doi: 10.1109/ICEMS.2019.8921689.

61- S. M. Dehghan, M. Mohamadian and E. Siefi, "Discontinuous energy pump source inverters," 2011 2nd Power Electronics, Drive Systems and Technologies Conference, Tehran, 2011, pp. 427-432, doi: 10.1109/PEDSTC.2011.5742459.

62- M. Kim et al., "A Single-Stage Three-Level AC/DC Converter for Wireless Power Transfer," 2019 IEEE Applied Power Electronics Conference and Exposition (APEC), Anaheim, CA, USA, 2019, pp. 3123-3128, doi: 10.1109/APEC.2019.8722248.

63- Y. Hsu, C. Ting, L. Hsu, J. Lin and C. C. Chen, "A Transient Enhancement DC–DC Buck Converter with Dual Operating Modes Control Technique," in IEEE Transactions on Circuits and Systems II: Express Briefs, vol. 66, no. 8, pp. 1376-1380, Aug. 2019, doi: 10.1109/TCSII.2018.2883889.

64- "Qi certified 3-coil 15 W wireless charger TX evaluation kit based on STWBC-MC" [Data brief].

Annex and Appendix

Annex A

Code of Arduino

```
#include <SoftwareSerial.h>
#include <Servo.h>
#include <Adafruit_Sensor.h>
#include <Adafruit_BNO055.h>
#include <NewPing.h>
Servo esc_signal;
Servo esc_signal1;
Servo servo1;
#define trig_pin A0 //analog input 1
#define echo_pin A1 //analog input 2
#define maximum_distance 200
int distance=100;
int comdata;
NewPing sonar(trig_pin, echo_pin, maximum_distance); //sensor function
int readPing()
  {
    delay(70);
    int cm=sonar.ping_cm();
    if (cm==0)
    {
      cm=250;
    }
    return cm;
  }
  int LookRight()
  {
    servo1.write(10);
    delay(500);
    int distance=readPing();
    delay(100);
    servo1.write(90);
    return distance;
  }
```

```
int LookLeft()
{
  servo1.write(170);
  delay(500);
  int distance=readPing();
  delay(100);
  servo1.write(90);
  return distance;
  delay(100);
}
void moveStop()
{
  esc_signal1.write(0);           //stop
  esc_signal.write(0);
}
void moveForward()
{
   esc_signal1.write(62);
  esc_signal.write(63);
}
void turnRight()
{
  esc_signal1.write(0);           //right
  esc_signal.write(63);
  delay(500);
}
void turnLeft()
{
  esc_signal1.write(62);           //left
  esc_signal.write(0);
  delay(500);
}
```

```
void setup()
{
  esc_signal.attach(9);  //Specify here the pin number on which the signal pin of ESC is connected.
  esc_signal.write(20); //ESC arm command. ESCs won't start unless input speed is less during initialization.
  esc_signal1.attach(10);  //Specify here the pin number on which the signal pin of ESC is connected.
  esc_signal1.write(20); //ESC arm command. ESCs won't start unless input speed is less during initialization.
servo1.attach(6);
  servo1.write(90);
  //delay(2000);
  distance=readPing();
  delay(100);
  distance=readPing();
  delay(100);
  distance=readPing();
  delay(100);
  distance=readPing();
  delay(100);
Serial.begin(9600);
}

void loop() {
  if (Serial.available()>0)
{
  comdata=Serial.read();
  if(comdata=='a')
  {

    esc_signal1.write(60);
    esc_signal.write(63);
  }
```

```
if(comdata=='b')
{
  esc_signal1.write(60);           //left
  esc_signal.write(0);


}
if(comdata=='c')
{
  esc_signal1.write(0);           //right
  esc_signal.write(63);
}
if(comdata=='d')
{
  esc_signal1.write(0);           //stop
  esc_signal.write(0);
}
if (comdata=='e')
{
  for(;comdata!='q';)
  {int distanceRight = 0;
  int distanceLeft = 0;
  delay(50);

  if (distance<=20)
  {
    esc_signal1.write(0);           //stop
    esc_signal.write(0);
    delay(300);
    distanceRight=LookRight();
    delay(300);
    distanceLeft=LookLeft();
    delay(300);
```

```
if (distance>=distanceLeft)
{
    esc_signal1.write(0);              //right
esc_signal.write(63);
esc_signal1.write(0);           //stop
esc_signal.write(0);
}
else
{
    esc_signal1.write(62);            //left
esc_signal.write(0);
esc_signal1.write(0);           //stop
esc_signal.write(0);
}
}
else{
    esc_signal1.write(62);   //forward
    esc_signal.write(63);
}
distance=readPing();
}
}
}


}
```

Annex B

Design of Wireless Power Transfer Circuit for Stable Voltage Output

Chen Ye
ISCTE-Instituto Universitário de Lisboa
IT-Instituto de Telecomunicações
SMU, Shanghai, China
Lisbon, Portugal
yechen913@gmail.com

Octavian Postolache
ISCTE-Instituto Universitário de Lisboa
IT-Instituto de Telecomunicações
Lisbon, Portugal
opostolache@lx.it.pt

Yongsheng Yang
Shanghai Maritime University
Shanghai, China
yangys_smu@126.com

Wangqiang Niu
Shanghai Maritime University
Shanghai, China
wqniu@shmtu.edu.cn

Abstract—**As a technology which can enhance charging safety and flexibility, wireless power transfer (WPT) was applied in some high-tech equipment, especially in aquatic drones, considering its complex charging environment. In order to improve the stability of wireless power transfer system voltage output while the relative position of two coils changing, a WPT circuit which can supply stable 12 V output voltage and current various with the distance changing between transmitting coil (Tx) and receiving coil (Rx) in a range from 5 mm to 30 mm is designed. To get the maximum transmission efficiency, the system is supposed to keep working at resonant frequency which is realized by frequency control chips for inverter in first side and rectifier in second side respectively. The detailed study of battery charging current versus coil distance is analyzed by simulation and experiment. In addition, the parameters of different circuit components such like capacity and inductance are fixed to obtain the resonance, which is determined by calculation and simulation. Meanwhile, the shape of coils is considered as well because it has clear affection on mutual inductance.**

Keywords—*Power Electronics, Wireless Power Transfer, RLC Circuit, Frequency Control, Voltage Stabilizing*

I. INTRODUCTION

With the great development of electric and electronic equipment age, people now have much higher requirements on electric power transmission to cope with various kinds of electricity consumption scenarios, particularly for those mobile electrical appliances which need to work for long time and are limited by battery performance. Then, WPT technology seems to be an ideal solution. Wireless power transfer firstly proposed by American scientist Nikola Tesla [1] in 1899 is a technology which enables devices to gain electric power from power source in a contactless way. However, this technology hasn't been widely applied until the last ten years and arouses more and more researchers' interests. Nowadays, WPT is used in robotics, small household appliances, human implant devices, mobile communication devices and electric vehicles, water and underwater unmanned vehicles, etc. Since the present battery life is still not long enough and devices need to be charged frequently, inductive WPT is able to improve safety and convenience of charging because it doesn't need any electrical contact compared with conventional wired power transfer [2]-[4].

However, WPT technology is still facing a lot of problems. For instance, WPT efficiency decreases significantly caused by Tx-Rx coils misalignment and the distance between them [5]. To solve the problem, different solutions were presented by researchers. In [6], a dipole-coil-based inductive power transfer (IPT) with a reflector, which adopts the variable switched capacitance under wide-range distance variation between Tx and Rx, is proposed. Unfortunately, in term of coil and circuit volume control, it is sacrificed for transmission performance so that the system lacks practicality. Furthermore, there're many other solutions focusing on coil shape or structure designing. For example, a transmitting coil with a tumbler structure is presented in [7] to improve lateral misalignment tolerance; also, [8] proposes a three-dimensional omnidirectional underwater wireless power transfer system to compensate angle misalignment.

On the other hand, some work on circuit resonance compensation plays an important role in WPT research such as [9] presenting a position-insensitive WPT based on nonlinear resonant circuits; [10] summarizing classic compensation topologies that realize constant-current or constant-voltage output as well as zero current switching (ZCS) or zero voltage switching (ZVS). It is also worth mentioning that

relay resonator can improve WPT efficiency stability too [11]-[13]. While in some cases, to achieve a high-level integration and a smaller power loss with a strong coupling, compensation on Rx can be eliminated [14]. In addition, frequency splitting phenomenon, which causes efficiency decrease at resonant frequency even when coupling coefficient is strong, is worth exploring [15].

Although there are various kinds of solutions which have been proposed in recent years, most of them are characterized by lack of simplicity and the whole volume of circuits are not compact enough [16]. Thus, it's usually hard to apply them into engineering practice. In this paper, integrated circuit chips XTK-801 and XTK-3170 are adopted to control operating frequency and series compensation circuits are soldered on two 4 cm * 2 cm PCB boards as Tx and Rx respectively. As a result, the presented WPT system can work steadily at 24 V input voltage, 36 W output power maximum and stable 12 V output voltage versus coupling coefficient change in a range from 0.2 to 0.8. The third part includes coil design and simulation. The fourth is an experimental and discussion part which is following by conclusions.

II. WPT Circuit Analysis

In this section, the coupling model [17] is considered to analyze components parameters and resonant frequency. The detail of components parameters determination for meeting the output demand is presented as well. In order to calculate more straightly, the whole model is simplified.

Circuit Modeling

The WPT circuit structure is composed of transmitting (primary) side and receiving (second) side, which is shown as Fig. 1. In first side, it mainly contains DC power supply, an inverter driven by an integrated frequency generator, resonant compensation circuit and Transmitting coil. In second side, a receiving coil, resonant compensation circuit, rectifier, stabilizer and resistant load are considered. The self-inductances of two coils are L_P and L_s respectivel, while M represents the mutual inductance.
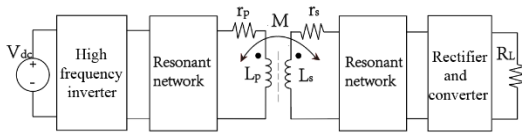
Fig. 1. A general WPT system diagram.

For convenience of analysis, DC voltage source and inverter can be seen as an AC voltage source. Simultaneously, the load, rectifier and stabilizer can be simplified into a resistant load while two coupling coils can be equivalent to a T-

shaped inductance structure after eliminating the mutual inductance as shown in Fig. 2. . In this work, series-series (S/S) compensation is utilized considering the necessity to have a constant voltage output and a simple construction.
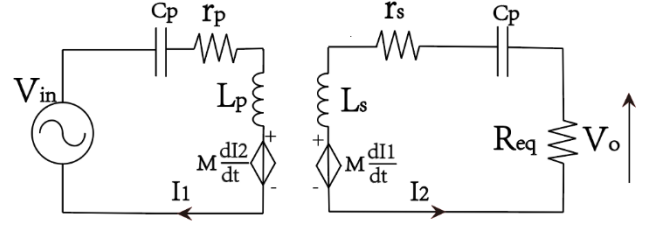
Fig. 2. A WPT system with S-S compensation.

a. Output Voltage Calculation and Dependances

In an S-S compensation topology as Fig. 2, the impedances Z_1 and Z_2 are defined as follows:

$$Z_1 = (L_p\omega - \frac{1}{\omega C_p})j + r_p \qquad (1)$$

$$Z_2 = (L_s\omega - \frac{1}{\omega C_s})j + r_s \qquad (2)$$

where C_P and C_S are the capacitances matching with L_P and L_s, ω is the operation frequency, r_p and r_s are the internal resistances in Tx and Rx respectively.

According to Kirchhoff's Law, the equation set is expressed as follows:

$$U_{in} = Z_1 I_1 + j\omega M I_2 \qquad (3)$$

$$U_o = Z_2 I_2 + j\omega M I_1 \qquad (4)$$

$$U_o = I_2 R_L \qquad (5)$$

where I_1 and I_2 are the currents through Tx and Rx respectively, U_{in} is the input voltage and R_L is the load resistance in the equivalent circuit.

Then, the relationship between I_1 and I_2, and the output voltage can be expressed as:

$$I_1 = \frac{I_2(R_L - Z_2)}{j\omega M} \qquad (6)$$

$$U_o = I_2 R_L = \frac{R_L U_{in} M \omega j}{(R_L - Z_2)Z_1 - M^2 \omega^2} \qquad (7)$$

where U_o is the output voltage across the load resistance. Substitute (1) and (2) into (7), assuming $C_p = C_s = C$, $r_p = r_s = r$ and $L_p = L_s = L$, which means $Z_1 = Z_2 = Z$, we can get:

$$U_o = j\omega M I_1 - r I_2 - (j\omega L - \frac{j}{\omega C})I_2 \qquad (8)$$

Then it can be considered that U_o is unrelated with R_L when $\omega_0 = \frac{1}{\sqrt{C(L-M)}}$, ω_0 - resonant

circular frequency. In addition, the output voltage can also be expressed as follows:

$$U_o = j\omega M I_1 - r I_2 \qquad (9)$$

In order to observe the effect of the mutual inductance variations on the output voltage, the partial derivation of the output voltage to the M can be expressed as follows:

$$\frac{\partial U_o}{\partial M} = \frac{\partial}{\partial M}(j\omega M I_1 - r I_2) = j\omega I_1 + j\omega M \frac{\partial I_1}{\partial M} - r\frac{\partial I_2}{\partial M} \qquad (10)$$

It can be observed that the change rate of U_o with M depends not only on M, but also on the variations of the current of the WPT on primary side.

AC-DC Converter Design

In order to convert AC voltage from receive side (Rx), an AC-DC converter is designed taking into account the following requirements. Usually, the output voltage in a WPT system is characterized by variations because the mutual inductance decreases when misalignment increasing. For small variations of M, the sensitivity can be expressed as follows:

$$S = \frac{\partial U_o(P_{out}, M)}{\partial M} \qquad (11)$$

where P_{out} is the output power. The sensitivity S can be used to optimize the stability of output voltage. Furthermore, the efficiency is another key performance index whose constraint can be expressed as follows:

$$\eta = \frac{P_{out}}{P_{in}} \geq \eta_{di} \qquad (12)$$

where η and η_{di} are the efficiency and design efficiency, P_{in} is the input power.

According to (12), desired voltage gain, thermal limits, switching and capacitor losses ought to be taken into account because these are the main factors influencing transmission efficiency. Furthermore, in order to stabilize the output voltage, a buck DC-DC converter is considered. In this case, a 36 W/ 85 kHz WPT system of which desired voltage gain is 0.5 and desired efficiency in an operation range is considered to be higher than 80%.

III. COIL DESIGN AND SIMULATION

To optimize the WPT system design, simulation of system coils is considered so that the coupling coefficient between Tx and Rx can be maximum. Further, we can obtain the condition of magnetic field when current flows through the coils via simulation.

In this work, planar spiral structure without magnetically permeable medium is considered because of its simplicity and smaller volume in plane compared with other structures like hemispherical and columnar spiral ones. Specifically, the inner and outer diameters of both coils are 30mm and 82 mm respectively with 15 turns winding. Besides, the diameter of the cable used to wind the coils is 1 mm.

The effect of coil coupling, the magnetic field situation between two coils was studied by simulation using Ansys Maxwell. Thus, 10 A current is set through the Tx and the result of simulation with and without misalignment is presented in Fig. 3. Furthermore, Fig. 4 (a) and (b) show the coupling coefficient change versus coil distance in range from 5 to 70 mm and misalignment in range of 0 to 40 mm respectively, which indicate that both distance and misalignment influence on coupling coefficient. Especially, it is also noticeable that the attenuation rate of the coupling coefficient versus coil distance is much bigger than that versus misalignment. In another word, the coupling coefficient is more sensitive to the distance change, so it's important to take it into consideration when designing WPT systems.

(a)

(b)
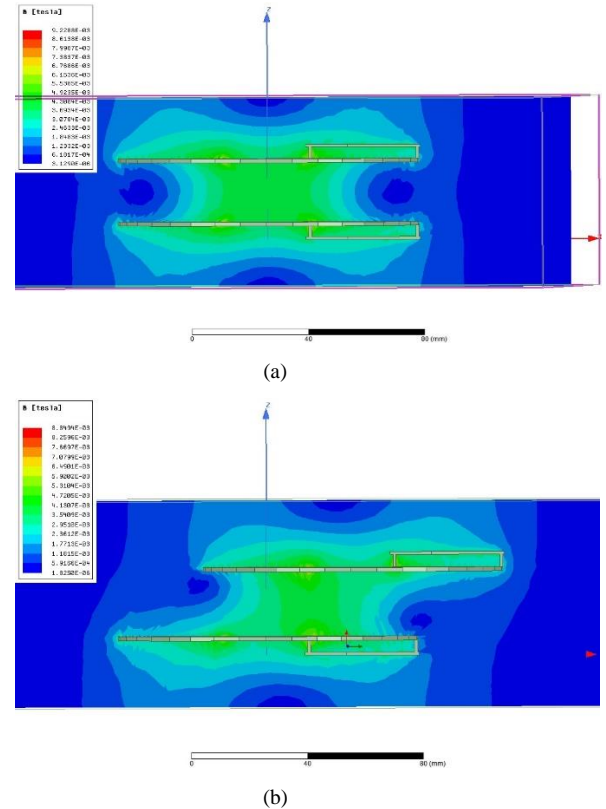
Fig. 3. Magnetic field. (a) Magnetic field without misalignment; (b) Magentic field with misalignment.

On the other hand, in order to optimize the parameters of whole circuit that is shown in Fig. 5 where XFG1 signal generator is used to emulate the integrated circuit (IC) to control the

switch of the buck DC-DC converter, both sides of WPT system are simulated by NI Multisim. The output voltage for different coupling coefficients which are 0.4, 0.6 and 0.8 is presented in Fig. 6 whcih indicates that the output voltage is stablized at about 12 V with various coupling coefficient.

(a)

(b)
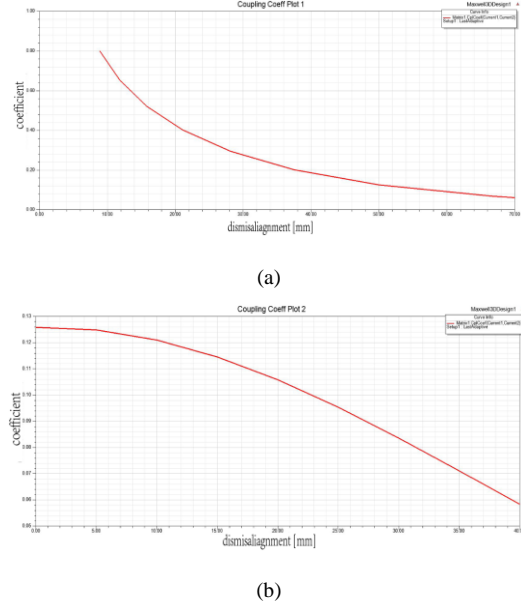
Fig. 4. Coupling coefficient. (a) versus coil distance; (b) versus misalignment

(a)

(b)

(c)

Fig. 6. Steady state output voltage under different coupling coefficient. (a),(b) and (c) show output voltages under coefficients which are 0.4, 0.6 and 0.8 respectively

Experimental Setup

In this case, an experiment is set up to verify the validation of the WPT system. The complete experiment devices are constituted by a DC voltage source (BK PRECISION 912B), a wireless charging module whose circuit design diagram is shown in Fig. 5 including transmitting and receiving sides, a KEITHLEY 2000 multimeter and an 11.1 V 2200 mAh Li-PO battery as the load. Fig. 7 is a photo of the whole experiment system.

Table I. PARAMETERS OF THE WPT SYSTEM

Components	Parameters	Values
Tx	L_p	14 μH
	C_p	70 μF
	ω_0	200 kHz
Rx	L_s	14 μH
	C_s	70 μF
	ω_0	200 kHz

During the experiment, the DC voltage source feeds 24 V voltage and 1.5 A current to the Tx of the WPT system. The experiment is processed in open circuit at first and then with load.

Fig. 5. Circuit diagram of both sides.

IV. EXPERIMENTAL RESULTS AND DISCUSSION

In previous section, both coil coupling and circuit simulation are given to indicate the relationship between relative coils position and coupling coefficient as well as the result of circuit design. In this section, it is focused on experiment description mainly composed of experiment devices, method and experiment results comparison analysis in different conditions.

Experiment Results Analysis

Open Circuit Situation: First, the voltage variations versus different colis distance and misaliagnment are researched. In this experiment, two coils are moved coaxially to change the distance between. Then, the coils are set to be 3 cm far and moved parallel to change the misalignment. The results are shown in Fig. 8. It can be seen that the voltage when coaxial stabilizes at about 12 V between 2.5-6.5 cm and decreases gradually while the distance is longer than 6.5 cm. However, the voltage with misalignment is stable when the misalignment is smaller than 5 cm and then attenuates severely. Considering the diameter of the coils is only 8.2 cm, not so large compared to the distance in the experiment, the voltage stabilization of the proposed WPT system is basically satisfied.
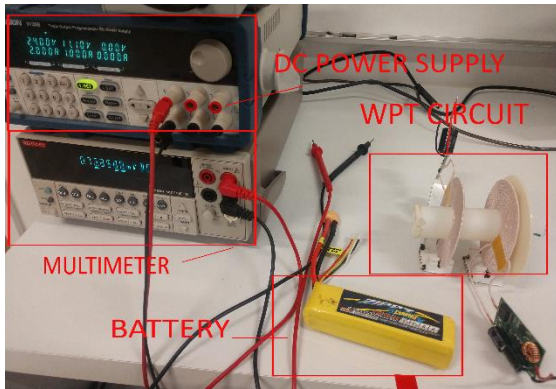
Fig. 7.   The experimental setup

Experiment with Load: When a 3C, 11.1V, 2200mAh LiPo battery is connected to the second side as the load, the current under different coupled index can be got. Thus, the power transmission efficiency can be derived by as follows:

$$\eta = \frac{P_{out}}{P_{in}} = \frac{U_{out}I_{out}}{U_{in}I_{in}} \tag{13}$$

In Fig. 8, it presents that the highest current 1.6 A and output power 19.4 W can be got when the distance is 0.5 cm and then it reduces as the distance keeps increasing. Meanwhile, the peak of power transmission efficiency reaches 80.6% at 0.5 cm and the trends of current, output power and power transmission curves going down with Tx-Rx distance increasing are basically the same, which corresponds to (13). Just in case the circuit of receiver is overloaded, the distance between coils can't be smaller than 0.5 cm. Since the voltage is stable at 12 V in the range of 0.5 to 7 cm, it means the output power and efficiency will decrease with the current. The errors in the experiment mainly are caused by measuring operation.
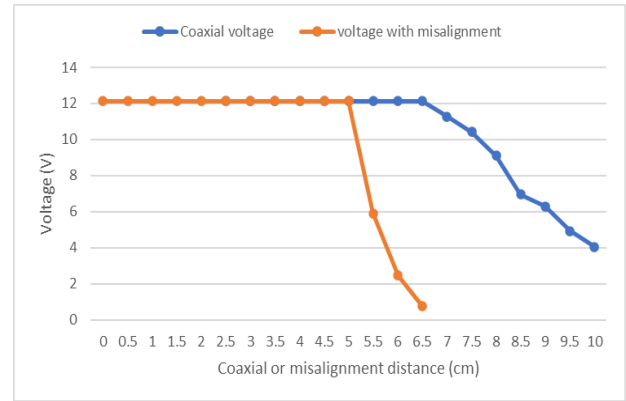
Fig. 8.   Open circuit voltage versus coils distance

The results of the current and power efficiency are shown in Fig. 9 and Fig. 10, separately.
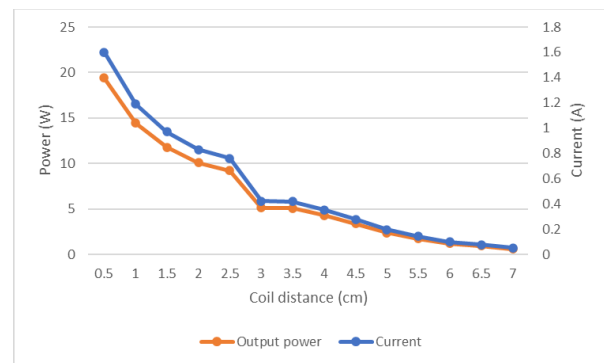
Fig. 9.   Current and output power value with battery load versus Rx-Tx coil distance
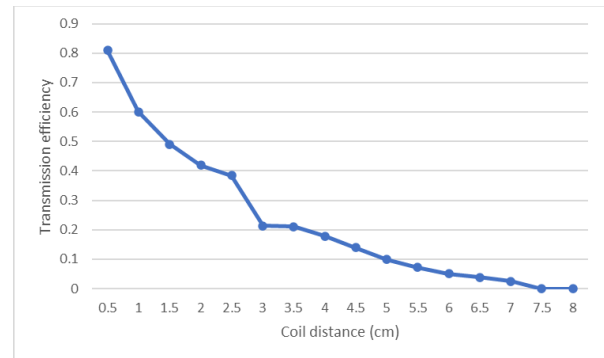
Fig. 10.   Power transmission efficiency versus Rx-Tx coil distance

V. CONCLUSION

This paper presents a WPT system which can supply a stable 12 V voltage and achieve around 80.6% highest power transmission efficiency with micro frequency control chips which reduces the circuit size obviously and makes it easier to be applied in small space. The simplified module of circuit is adopted to analyze the system. The experiment is brought out to prove the validation of the system. The results show that the proposed system has a good performance in terms of reducing output voltage

sensitivity to misalignment and coil distance change.

As the future work, the characteristics of WPT system for aquatic drone development will be developed, which includes eddy current loss in various kinds of liquid medium, in order to improve performance of underwater WPT charging station for underwater automatic vehicles (UAVs).

VI. ACKNOWLEDGMENT

VII. REFERENCES

[1] A. Rajvanshi,"Nikola Tesla- The Creator of Electric Age," Resonance, March 2007.

[2] S. Lukic, Z. Pantic,"Cutting the Cord: Static and Dynamic Inductive Wireless Charging of Electric Vehicles," IEEE Electrification Magzine, pp. 57-64, 2013.

[3] S. Hui, W. Ho,"A New Generation of Universal Contactless Battery Charging Platform for Portable Consumer Electronic Equipment," IEEE Trans. on Power Electron., vol. 20, no. 3, pp: 620-627, 2005.

[4] B. Choi, J. Nho, H. Cha, et al.,"Design and Implementation of Low-profile Contactless Battery Charger Using Planar Printed Circuit Board Wingdings as Energy Transfer Device," IEEE Trans. on Industrial Electron., vol. 51, no. 1, pp. 140-147, 2004.

[5] S. Lee, G. Choi, S. Choi, T. Nguyen, and T. Rim," Wide-Range Adaptive IPT Using Dipole-Coils With a Reflector by Variable Switched Capacitance," IEEE Trans. on Power Electron., vol. 32, no. 10, pp. 8054-8070, Oct. 2017.

[6] S. Ding, W. Niu, and W. Gu," Lateral Misalignment Tolerant Wireless Power Transfer with a Tumbler Mechanism," IEEE Access, vol. 7, pp. 125091-125100, August 2019.

[7] Z. He, Y. Wang, L. Ding, and X. Nie," Research on Three-Dimensional Omnidirectional Wireless Power Transfer System for Subsea Operation," OCEANS 2017-Aberdeen, UK, June 1017.

[8] O. Abdelatty, X. Wang, and A. Mortazawi," Position-Insensitive Wireless Power Transfer Based on Nonlinear Resonant Circuits," IEEE Trans. on Microwave Theory and Techniques., vol. 67, no. 9, pp. 3844-3855, March 2019.

[9] W. Zhang, and C. Mi," Compensation Topologies of High-Power Wireless Power Transfer Systems," IEEE Trans. on Vehicular Technology., vol. 65, no. 6, pp. 4768-4778, June 2016.

[10] J. Lee, K. Lee, and D. Cho," Stability Improvement of Transmission Efficiency based on Relay Resonator in Wireless Power Transfer System," IEEE Trans. on Power Electron., vol.32, no. 5, pp. 3297-3300, May 2017.

[11] W. Niu, J. Wang, J. Chu, W. Gu," Optimal single relay position of a 3-coil wireless power transfer system," The Journal of Engineering, vol. 2016, no. 7, pp. 249-252, July 2016.

[12] J. Agbinya, and H. Nguyen," Principles and Applications of Frequency Splitting in Inductive Communications and Wireless Power Transfer Systems," Wireless Personal Communications, vol. 107, pp. 987-1017, April 2019.

[13] Y. Zhang, T. Kan, Z. Yan, Y. Mao, Z. Wu, and C. Mi," Modeling and Analysis of Series-None Compensation for Wireless Power Transfer Systems with a Strong Coupling," IEEE Trans. on Power Electron., vol. 34, no. 2, pp.1209-1215, Feb. 2019.

[14] A. Ramezani, S. Farhangi, H. Eini, B. Farhangi, R. Rahimi, and G. Moradi," Optimized LCC-Series Compensated Resonant Network for Stationary Wireless EV Charger," IEEE Trans. on Industrial Electron., vol. 66, no. 4, pp. 2756-2765, June 2018.

[15] W. Niu, J. Chu, W. Gu, A. Shen," Exact Analysis of Frequency Splitting Phenomena of Contactless Power Transfer Systems," IEEE Trans. on Circuits and Systems, vol. 60, no. 6, pp. 1670-1677, June 2013.

[16] K. Mude, K. Aditya,"Comprehensive review and analysis of two-element resonant compensation topologies for wireless inductive power transfer systems," CMP, vol. 5, no. 12, pp.14-31, June 2019.

[17] G. Qiu,"Circuit," China: Hingher Education Press, June 2006.